# Singlet fission in covalent dimers of methylene-locked 1,3-diphenyl-isobenzofuran: semiclassical simulations of nonadiabatic dynamics

**Davide Accomasso, Giovanni Granucci, and Maurizio Persico**

Università di Pisa, Dipartimento di Chimica e Chimica Industriale,
via Moruzzi 13, 56124 Pisa, Italy

## Supporting Information

## S1 Computational methods

Table S0: Transition energies (in eV) for the $S_1$, $S_2$, $S_3$, $T_1$ and $T_2$ electronic states of 1,3-diphenyl-isobenzofuran (DPBF), i.e. the parent compound of ML-DPBF.

| Method | Vertical | | | | | Adiabatic | |
|---|---|---|---|---|---|---|---|
| | $S_1$ | $S_2$ | $S_3$ | $T_1$ | $T_2$ | $S_1$ | $T_1$ |
| Experimental | 3.01[a] | 3.67[a] | 3.86[a] | - | - | 2.76[b] | 1.41[c]; 1.48[d] |
| RI-CC2/TZVPP[e] | 3.22 | 4.14 | 4.29 | 2.05 | 3.53 | 2.98 | 1.72 |
| B3LYP/6-311G(d,p) | 2.91[f] | 3.96[f] | 3.97[f] | 1.78[g] | 3.11[f] | 2.66[f] | 1.44[g] |

[a] Absortion spectrum in 3-methylpentane at 77 K, band maximum [1].
[b] Fluorescence spectrum in cyclohexane, 0-0 transition [1].
[c] Electron energy loss spectroscopy in a solid film [1].
[d] Determined by sensitization in benzene [2].
[e] Computed with the RI-CC2/TZVPP method, using the point group $C_2$ [1].
[f] Computed in the present work at the TD-DFT level (B3LYP/6-311G(d,p)), using the point group $C_2$.
[g] Computed in the present work at the unrestricted open-shell DFT level (B3LYP/6-311G(d,p)), using the point group $C_2$.

### S1.1 Additional Lennard-Jones interaction potential between chromophores

To better account for dispersion and repulsion interactions between atoms of different chromophores in the covalently bound dimers under study, interatomic potential energy terms of Lennard-Jones (LJ) type were added to the state energies computed at the R-AM1/FOMO-CASCI(4,8) level. In particular, the state energies were corrected using the following additional LJ potential

$$V_{LJ} = \sum_{i\in A}\sum_{i\in B} 4\,\epsilon_{ij}\left[\left(\frac{\sigma_{ij}}{R_{ij}}\right)^{12} - \left(\frac{\sigma_{ij}}{R_{ij}}\right)^{6}\right] \tag{S1}$$

where $i$ and $j$ run over the carbon and oxygen atoms of chromophore A and B, respectively, $R_{ij}$ is the distance between atoms $i$ and $j$, and $\epsilon_{ij}$ and $\sigma_{ij}$ are parameters for atom pair $ij$. The latter are geometric means of atomic parameters, i.e. $\epsilon_{ij} = \sqrt{\epsilon_i \epsilon_j}$ and $\sigma_{ij} = \sqrt{\sigma_i \sigma_j}$. In our calculations, the atomic parameters $\{\epsilon_i\}$ and $\{\sigma_i\}$ were selected from the ones defining the OPLS-AA force field [3]. In particular, an OPLS-AA atom type was assigned to each carbon (C) and oxygen (O) atom of the ML-DPBF chromophore, as reported in Table S1.

Table S1: Atom types and corresponding Lennard-Jones (LJ) parameters of the OPLS-AA force field [3] selected to define the corrective potential term (Eq. S1) included in the electronic structure calculations for the covalently bound dimers of ML-DPBF.

| Atoms | Atom type | $\epsilon$ (kcal) | $\sigma$ (Å) |
|---|---|---|---|
| All carbons except the -$CH_2$- ones | Aromatic C (90) | 0.070 | 3.550 |
| Carbons of -$CH_2$- bridges | Alkane -$CH_2$- (81) | 0.066 | 3.500 |
| Oxygen | Furan O (507) | 0.140 | 2.900 |

## S1.2 Calculation of an effective electronic Hamiltonian matrix

Given a set of $N$ electronic wave functions[1] $\{\Phi_i\}$, one may be interested to estimate the effect of a subset of these states, typically the $N-M$ higher energy ones ($M < N$) which define an "outer space", on the electronic Hamiltonian matrix elements which couple the other $M$ states, which span a "model space". This can be achieved using either a perturbative approach, such as the quasi-degenerate perturbation theory, or a variational one [4, 5]. In the present work, we adopt the variational approach and we proceed as follows.

After diagonalizing the electronic Hamiltonian matrix in the initial $N$-dimensional space, we project the eigenfunctions $\{\Psi_i | i = 1, 2, \ldots, N\}$ onto the model space (of dimension $M < N$). Then, we select the $M$ projections $\{\widetilde{\Psi}_i\}$ with the largest norm, together with their corresponding eigenvalues $\{E_i | i = 1, 2, \ldots, M\}$. Since the selected projections are in general not orthogonal, we orthogonalize them using the Löwdin method [6] and employ the functions obtained $\{\widetilde{\Psi}_i^{\perp}\}$ to define a so-called "effective Hamiltonian":

$$\hat{H}_{el}^{eff} = \sum_{i=1}^{M} |\widetilde{\Psi}_i^{\perp}\rangle E_i \langle\widetilde{\Psi}_i^{\perp}| \tag{S2}$$

where we have used the spectral decomposition formula. Notice that the effective Hamiltonian constructed with the orthogonalized functions $\{\widetilde{\Psi}_i^{\perp}\}$ is hermitian, while it would not be so if we employed the non-orthogonal projections $\{\widetilde{\Psi}_i\}$. Since $\widetilde{\Psi}_i^{\perp} = \sum_{j=1}^{M} \Phi_j \, \widetilde{C}_{ji}^{\perp}$, the effective Hamiltonian matrix in the basis of the model space functions $\{\Phi_i | i = 1, 2, \ldots, M\}$ is given by:

$$\left(H_{el}^{eff}\right)_{jk} = \sum_{i=1}^{M} \widetilde{C}_{ji}^{\perp} \, E_i \, \widetilde{C}_{ki}^{\perp}. \tag{S3}$$

In the construction of the effective Hamiltonian matrices for dimers **D1** and **D2** (see Section 3, in the main text, and Table S4), the model space is defined by either the excitonic states $S_1^*$, $S_2^*$ and $TT$, or the diabatic states $S_1S_0$, $S_0S_1$ and $TT$, while the outer space is spanned by the $CT_1$, $CT_2$, $S_1^{**}$ and $S_2^{**}$ states (excitonic basis), or by $A^-B^+$, $A^+B^-$, $S_2S_0$ and $S_0S_2$ (diabatic basis). Therefore, the effective coupling between $S_1^*$ (or $S_2^*$) and $TT$ includes both the $S_1^*$-$TT$ (or $S_2^*$-$TT$) direct electronic coupling and the contributions from the higher energy states $CT_1$, $CT_2$, $S_1^{**}$ and $S_2^{**}$.

[1] They may be determinants, single configurations or multi-configurational wave functions as the diabatic or excitonic states employed to analyse our dynamics simulations (see the main text).

## S1.3 Direct trajectories with surface hopping

The simulations of nonadiabatic dynamics presented in Section 3.2 (see the main text) were performed using the direct trajectories with surface hopping (DTSH) method described in Ref. [7]. In such approach, the quantum wavepacked dynamics is approximated using an ensemble of independent semiclassical trajectories. In each trajectory, the nuclei evolve in time according to the Newton's equation of classical mechanics:

$$M_\alpha \, \ddot{Q}_\alpha(t) = -\frac{\partial V(\mathbf{Q}(t))}{\partial Q_\alpha} \tag{S4}$$

where $\mathbf{Q}$ is the collection of nuclear coordinates, i.e. $\mathbf{Q} = \{Q_\alpha\}$, $\{M_\alpha\}$ are nuclear masses, and $V$ is the potential energy for the nuclear motion. In the DTSH method, Eq. S4 is integrated using a Verlet-type algorithm [8]. At each integration time step, the nuclear trajectory is driven by one adiabatic potential energy surface (PES), i.e. $V(\mathbf{Q}) = E_k(\mathbf{Q})$, where $E_k(\mathbf{Q})$ is the $k$-th eigenvalue of the electronic Hamiltonian $\hat{\mathcal{H}}_{el}(\mathbf{q};\mathbf{Q})$, corresponding to the eigenstate $\Phi_k^{(A)}(\mathbf{q};\mathbf{Q})$, in which $\mathbf{q}$ is the collection of electronic coordinates. In the DTSH method, the adiabatic PESs and wavefunctions, $\{E_k\}$ and $\{\Phi_k^{(A)}\}$, are computed by the semiempirical FOMO-CI method described in Section S1.4. To account for nonadiabatic effects, the nuclear and electronic motions are coupled by sudden hops between PESs. In particular, during the time propagation of a semiclassical trajectory, the potential energy $V(\mathbf{Q})$, driving the nuclear motion, may change from $E_k(\mathbf{Q})$ to $E_l(\mathbf{Q})$, according to a chosen surface hopping algorithm.

Several surface hopping treatments have been proposed (see Ref. [9, 10] for a general overview). In the DTSH method, the "fewest switches" surface hopping (FSSH) algorithm, proposed by Tully in 1990 [11], is used. Such algorithm, which represents the most commonly used surface hopping scheme, minimizes the number of state switches required to distribute the nuclear trajectories on the electronic states, according to the computed transition probabilities. The FSSH algorithm requires to evolve in time the electronic wavefunction $\Psi_{el}$ according to a time-dependent Schrödinger equation (TDSE) only for the electrons:

$$i\hbar \, \frac{\mathrm{d}\, \Psi_{el}(\mathbf{q},t;\mathbf{Q}(t))}{\mathrm{d}t} = \hat{\mathcal{H}}_{el}(\mathbf{q};\mathbf{Q}(t)) \, \Psi_{el}(\mathbf{q},t;\mathbf{Q}(t)) \tag{S5}$$

where $\mathbf{Q}(t)$ is the classical nuclear trajectory. In particular, $\Psi_{el}$ is expandend in a basis of adiabatic states $\{\Phi_l^{(A)}\}$:

$$\Psi_{el}(\mathbf{q},t;\mathbf{Q}(t)) = \sum_l \, a_l(t) \;\; \Phi_l^{(A)}(\mathbf{q};\mathbf{Q}(t)). \tag{S6}$$

Substitution of Eq. S6 into Eq. S5, followed by multiplication of both sides by $\Phi_k^{(A)*}$ and integration over the electronic coordinates $\mathbf{q}$, yields:

$$\dot{a_k}(t) = -i\frac{E_k}{\hbar} a_k(t) - \sum_{l(\neq k)} a_l(t) \left[ \sum_\alpha \dot{Q}_\alpha \, g_{kl}^{(\alpha)} \right] \tag{S7}$$

where $g_{kl}^{(\alpha)}$ is the derivative coupling between $\Phi_k^{(A)}$ and $\Phi_l^{(A)}$, i.e. $g_{kl}^{(\alpha)} = \langle \Phi_k^{(A)} | \frac{\partial}{\partial Q_\alpha} | \Phi_l^{(A)} \rangle$. Since the (approximate) solution of Eq. S7 based on the adiabatic representation is prone to inaccuracy in regions of weakly avoided curve crossings or conical intersections, in the DTSH method Eq. S7 is solved using a local diabatization algorithm [7],

inherently stable in quasi-degenerate situations. The latter is based on a "locally diabatic" representation, i.e. a set of electronic states which are diabatic along the nuclear trajectory under consideration. In such algorithm, the time-dependent coefficients in the adiabatic basis, $\mathbf{a}(t)$, at the end of the time step ($t = \Delta t$) are obtained from the ones at the beginning of the time step ($t = 0$), using the following formula:

$$\mathbf{a}(\Delta t) = \mathbf{T}^{\dagger}(\Delta t)\; e^{-\frac{i}{\hbar}\mathbf{Z}\Delta t}\; \mathbf{a}(0) \tag{S8}$$

with

$$\mathbf{Z} = \frac{1}{2}\big[\mathbf{E}(0) + \mathbf{T}(\Delta t)\; \mathbf{E}(\Delta t)\; \mathbf{T}^{\dagger}(\Delta t)\big] \tag{S9}$$

where $\mathbf{T}$ is the transformation matrix from the adiabatic basis $\{\Phi_k^{(A)}\}$ to the basis of locally diabatic states, and $\mathbf{E}$ is the diagonal matrix of adiabatic electronic energies. The transformation matrix $\mathbf{T}$ at time $\Delta t$ is computed by Löwdin orthogonalization [6] of the columns of the overlap matrix $\mathbf{S}$ between the adiabatic states at $t = 0$ and $t = \Delta t$:

$$S_{kl} = \langle \Phi_k^{(A)}(0) | \Phi_l^{(A)}(\Delta t) \rangle. \tag{S10}$$

As we can see from Eq. S8 and S9, the local diabatization algorithm does not require the calculation of the derivative (or nonadiabatic) couplings between adiabatic states. Moreover, the high stability of such algorithm allows to use a larger time step compared to integration algorithms based on the adiabatic representation [12].

Once the time-dependent coefficients $\mathbf{a}(\Delta t)$ are obtained, the FSSH transition probability from the current adiabatic state $\Phi_k^{(A)}$ to state $\Phi_l^{(A)}$, at the end of a time step $\Delta t$, is defined as follows:

$$P_{k\to l} = max\left\{0, \frac{B_{kl}\; \Delta t}{|a_k(0)|^2}\right\} \tag{S11}$$

where $B_{kl}$ is the contribution of state $l$ to the variation of the population of state $k$ in the time step $\Delta t$:

$$\frac{|a_k(\Delta t)|^2 - |a_k(0)|^2}{\Delta t} = -\sum_{l(\neq k)} B_{kl}. \tag{S12}$$

If $B_{kl} > 0$, then $P_{k\to l} = \frac{B_{kl}\; \Delta t}{|a_k(0)|^2}$; while if $B_{kl} < 0$, then $P_{k\to l} = 0$ (see Eq. S11). In the adiabatic basis, $B_{kl}$ is given by:

$$B_{kl} = 2\; \mathcal{R}\{G_{kl}\; \rho_{lk}\} \tag{S13}$$

with

$$G_{kl} = \langle \Phi_k^{(A)} | \dot{\Phi}_l^{(A)} \rangle = \sum_{\alpha} g_{kl}^{(\alpha)}\; \dot{Q}_{\alpha} \tag{S14}$$

$$\rho_{lk} = a_l\; a_k^{*} \tag{S15}$$

where $\mathcal{R}$ stands for the real part, and $\rho_{lk}$ is the electronic density matrix element between states $\Phi_k^{(A)}$ and $\Phi_l^{(A)}$. Note that $\rho_{kk} = |a_k(t)|^2$ is the probability of state $k$ at time $t$, computed along a given trajectory.

If the local diabatization algorithm is used to integrate the electronic TDSE, the derivative (or nonadiabatic) couplings between adiabatic states are not computed and the FSSH transition probabilities cannot be directly evaluated using Eq. S11 and S13. Different ways were proposed to define FSSH transition probabilities in combination

with the local diabatization algorithm [7, 13, 14]. In the simulations presented in Section 3.2 we used the following definition (proposed for the first time in Ref. [14]):

$$P_{k\to l} = max\left\{0, \frac{\rho_{kk}(0) - \rho_{kk}(\Delta t)}{\rho_{kk}(0)}\right\} \frac{|T_{kl}(\Delta t)|\sqrt{\Delta\rho_{ll}}}{\sum_{j(\neq k)} |T_{kj}(\Delta t)|\sqrt{\Delta\rho_{jj}}} \tag{S16}$$

with

$$\Delta\rho_{ll} = max\{0, \rho_{ll}(\Delta t) - \rho_{ll}(0)\}. \tag{S17}$$

Eq. S16 takes into account both the variations of the populations of states $k$ and $l$, and the coupling between them, which is proportional to the overlap $\langle\Phi_k^{(A)}(0)|\Phi_l^{(A)}(\Delta t)\rangle$, and hence to the matrix element $T_{kl}(\Delta t)$. Moreover, Eq. S16 has the following good features: (i) it provides the exact transition propabilities for the case of two states, (ii) it deals correctly with non interacting or weakly interacting states, and (iii) it ensures a reasonable partition of the variation of the current state population in the time step $\Delta t$.

Once the transitions probabilities from the current state $k$ to all the other state $l$ are computed using Eq. S16, a random number $r_t \in [0, 1]$ is extracted. Then, two cases are possible. If $r_t$ is such that

$$\sum_{j=1}^{l-1} P_{k\to j} < r_t \leq \sum_{j=1}^{l} P_{k\to j} \tag{S18}$$

a hop from state $k$ to state $l$ may occur (see below), otherwise, i.e. if

$$\sum_{j} P_{k\to j} < r_t \leq 1, \tag{S19}$$

no hop during the current time step is done. In the former case (Eq. S18), the $k \to l$ hop is done only if the conservation of the total energy can be satisfied. In particular, if the nuclear kinetic energy $T_n$ is larger than (or at least equal to) the sudden variation in the potential energy $E_l - E_k$ required by the hop, i.e. $T_n \geq E_l - E_k$, the $k \to l$ hop is done. On the contrary, if $T_n < E_l - E_k$, the hop is rejected. When the $k \to l$ hop occurs, the nuclear velocities are rescaled to compensate for the sudden variation in the potential energy $E_l - E_k$. If the derivative couplings $\{g_{kl}^{(\alpha)}\}$ are available, such rescaling is usually done in the direction of the $\mathbf{g}_{kl}$ vector. In the present work, wherein the local diabatization algorithm is used and the derivative couplings are not computed, the nuclear velocities are rescaled in the direction of the vector of momenta.

In Figure S0 we provide a schematic representation of the procedure required to propagate in time a surface hopping trajectory according to the DTSH method employed in the present work.

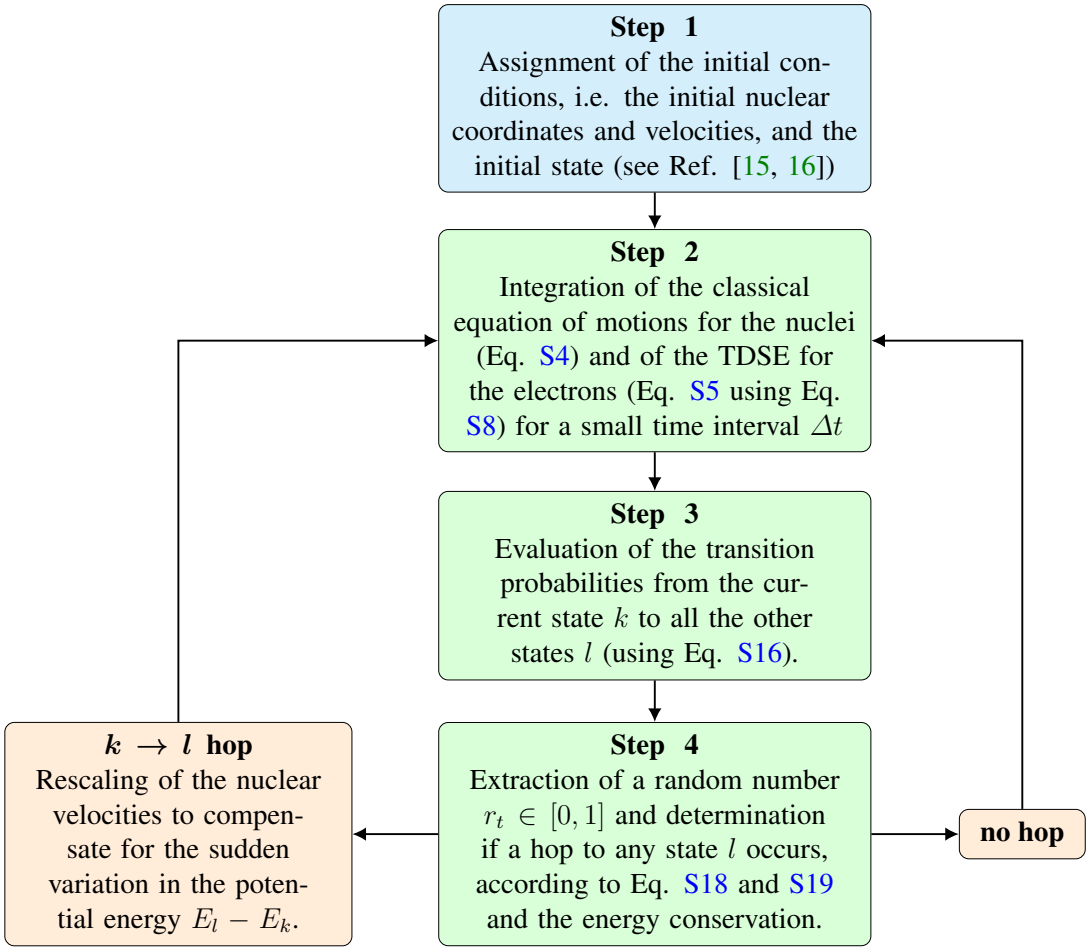


Figure S0: Schematic representation of the time propagation of a semiclassical surface hopping trajectory, according to the direct trajectories with surface hopping (DTSH) method employed in the present work.

One of the main drawbacks of the "fewest switches" surface hopping (FSSH) method is its unsuitable treatment of quantum decoherence effects. The term "quantum decoherence" is used to indicate the decay to zero of the off-diagonal elements of the density matrix of a system, which in turn are called "coherences". Using a fully quantum mechanical description of a molecular system based on the Born-Huang (BH) expansion of the wavefunction [17]

$$\Psi(\mathbf{Q}, \mathbf{q}, t) = \sum_j \Theta_j(\mathbf{Q}, t)\, \Phi_j^{(A)}(\mathbf{q}; \mathbf{Q}), \tag{S20}$$

the electronic density matrix is given by

$$\rho_{kl}^{(BH)} = \langle \Phi_k^{(A)} | \Psi \rangle_{\mathbf{q}} \langle \Psi | \Phi_l^{(A)} \rangle_{\mathbf{q}} = \Theta_k(\mathbf{Q})\, \Theta_l^*(\mathbf{Q}) \tag{S21}$$

where the subscripts $\mathbf{q}$ indicate that the integrations are performed on the electronic coordinates. Since the wavepackets $\Theta_k(\mathbf{Q})$ and $\Theta_l(\mathbf{Q})$ travel on two different PESs, namely $E_k(\mathbf{Q})$ and $E_l(\mathbf{Q})$, they may get far from each other in the space of the nuclear coordinates $\mathbf{Q}$. In this case, $\rho_{kl}^{(BH)}$ tends to vanish, and so do all the coupling matrix elements between $\Theta_k(\mathbf{Q})$ and $\Theta_l(\mathbf{Q})$. The latter can vanish even when $\Theta_k(\mathbf{Q})$ and $\Theta_l(\mathbf{Q})$ overlap in the $\mathbf{Q}$ coordinate space, but are well separated in the space of nuclear momenta $\mathbf{P}$, i.e. one is fast and the other is slow or they travel in different directions.

As a result, in both cases discussed above no transfer of population between $\Theta_k(\mathbf{Q})$ and $\Theta_l(\mathbf{Q})$ will occur any more.

In the FSSH method, for each trajectory the same representative point in the phase space is used to propagate in time the electronic coefficients $\mathbf{a}(t)$ of all the electronic states, i.e. the propagation of the electronic TDSE is fully coherent. Therefore, the FSSH electronic density matrix (Eq. S15) behaves differently from the fully quantum one (Eq. S21). In particular, an off-diagonal elements of the FSSH electronic density matrix (Eq. S15) can vanish only if at least one of the coefficients $a_l$ and $a_k$ is zero. Even if the trajectory explores for a long time regions where the coupling between $\Phi_k^{(A)}$ and $\Phi_l^{(A)}$ is negligible, the FSSH algorithm does not necessarily features the decay of $\rho_{kl}$. Then, if the trajectory, carrying incorrect $\mathbf{a}(t)$, enters an interaction region, it may undergo incorrect hops between PESs, leading to unphysical effects.

Several schemes have been proposed to properly include quantum decoherence in the FSSH algorithm [18–20]. In such approaches, the general strategy consists of introducing a collapse of the electronic wavefunction on the current state $k$, i.e. enforcing $a_k \to 1$ and $a_l \to 0$, $\forall l \neq k$, within an appropriate time interval. In the surface hopping simulations presented in Section 3.2 we used a scheme based on the evaluation of the overlap between frozen gaussian wavepackets, which are propagated in time in an approximate way as described in details in Ref. [20].

## S1.4 Semiempirical FOMO-CI method

In the dynamics simulations presented in Section 3 (see the main text), the PESs on which the nuclei evolve are computed using a configuration interaction method based on floating occupation molecular orbitals (FOMO-CI), in its semiempirical variant [7, 21]. Such methodology consists of two main steps. First, the molecular orbitals (MOs) are computed through a self-consistent field (SCF) procedure in which the MOs are partitioned, on the basis of their energetic ordering, into inactive, active and virtual: the inactive orbitals are doubly occupied, the virtual MOs are unoccupied and the active ones have fractional, and possibly "floating" (i.e. variable, with respect to the molecular geometry), occupations. In the latter case, the occupation numbers are defined as follows

$$O_k = \frac{\sqrt{2}}{\sqrt{\pi} w} \int_{-\infty}^{\epsilon_F} e^{-\frac{(\epsilon - \epsilon_k)^2}{2w^2}} d\epsilon \tag{S22}$$

where $\epsilon_k$ is the energy of the $k$-th MO, $\epsilon_F$ is the the Fermi level, determined by imposing that the sum of the occupation numbers is equal to the total number of electrons, i.e. $N_{el} = \sum_k O_k$, and $w$ is the orbital energy width, an arbitrarily chosen parameter which determines the spread of electronic population below and above the Fermi level. Such occupation numbers are used to define the 1-electron density matrix $\mathbf{D}$, which in turn is used to construct the Fock matrix $\mathbf{F}$ in the SCF procedure:

$$D_{ij} = \sum_k O_k \, C_{ik} \, C_{jk} \tag{S23}$$

$$\mathbf{F} = \mathbf{h} + \mathbf{G}(\mathbf{D}) \tag{S24}$$

where $C_{ik}$ is the coefficient of the $k$-th MO for the $i$-th atomic orbital basis function, $\mathbf{h}$ is the one-electron integrals part of $\mathbf{F}$ and $\mathbf{G}$ is the matrix of two-electron integrals (Coulomb and exchange). Note that, in this FOMO-SCF procedure, the occupation

numbers of Eq. S22 are self-consistently determined according to the orbital energies $\{\epsilon_k\}$, obtained by diagonalization of $\mathbf{F}$ at each SCF iteration.

Once the MOs are computed through the FOMO-SCF step, they are employed to perform a subsequent configuration interaction (CI) calculation. In the present work, the CI space is truncated by doing a CASCI calculation, i.e. a full CI within the space of the active MOs. This variant of the FOMO-CI method can be viewed as a convenient substitute for the complete active space self-consistent field (CASSCF) method. From the CASCI step, the energies and wavefunctions of the low-lying adiabatic electronic states are obtained. In case of a surface hopping trajectory or a geometry optimization, the analytical derivatives of the FOMO-CI electronic energies with respect to the nuclear coordinates are also computed as described in Ref. [21].

In the semiempirical variant of the FOMO-CI technique, employed in the present work, the elements of the Fock matrix for the SCF step, together with the ones of the electronic Hamiltonian matrix in the determinant basis for the CI procedure, are evaluated in the framework of the selected semiempirical method. In particular, the integrals are either determined directly from experimental data or computed using analytical formulas or suitable parametric expressions. In the present work we adopted the Austin Model 1 (AM1) semiempirical model [22] with parameters specifically reoptimized for our investigated systems. In general, such semiempirical FOMO-CI methodology allows to take into account both the static electron correlation, by the CI procedure, and the dynamical one, through the semiempirical parameters, which can be adjusted in order to reproduce experimental or ab initio results for the particular system under study. Moreover, the FOMO-SCF procedure allows the MOs to adapt smoothly to changes of the nuclear geometry, which is an indispensable requirement if the MOs are to be used in molecular dynamics simulations. This is particularly important in case of single bond breaking or double bond twisting processes, in which the problem of orbital degeneracy has to be tackled. Furthermore, the partial optimization of some MOs above the Fermi level, which are partially filled, generally improves the description of excited states.

# S2 Stacked dimers D1 and D2

## S2.1 Ground state thermal equilibrations

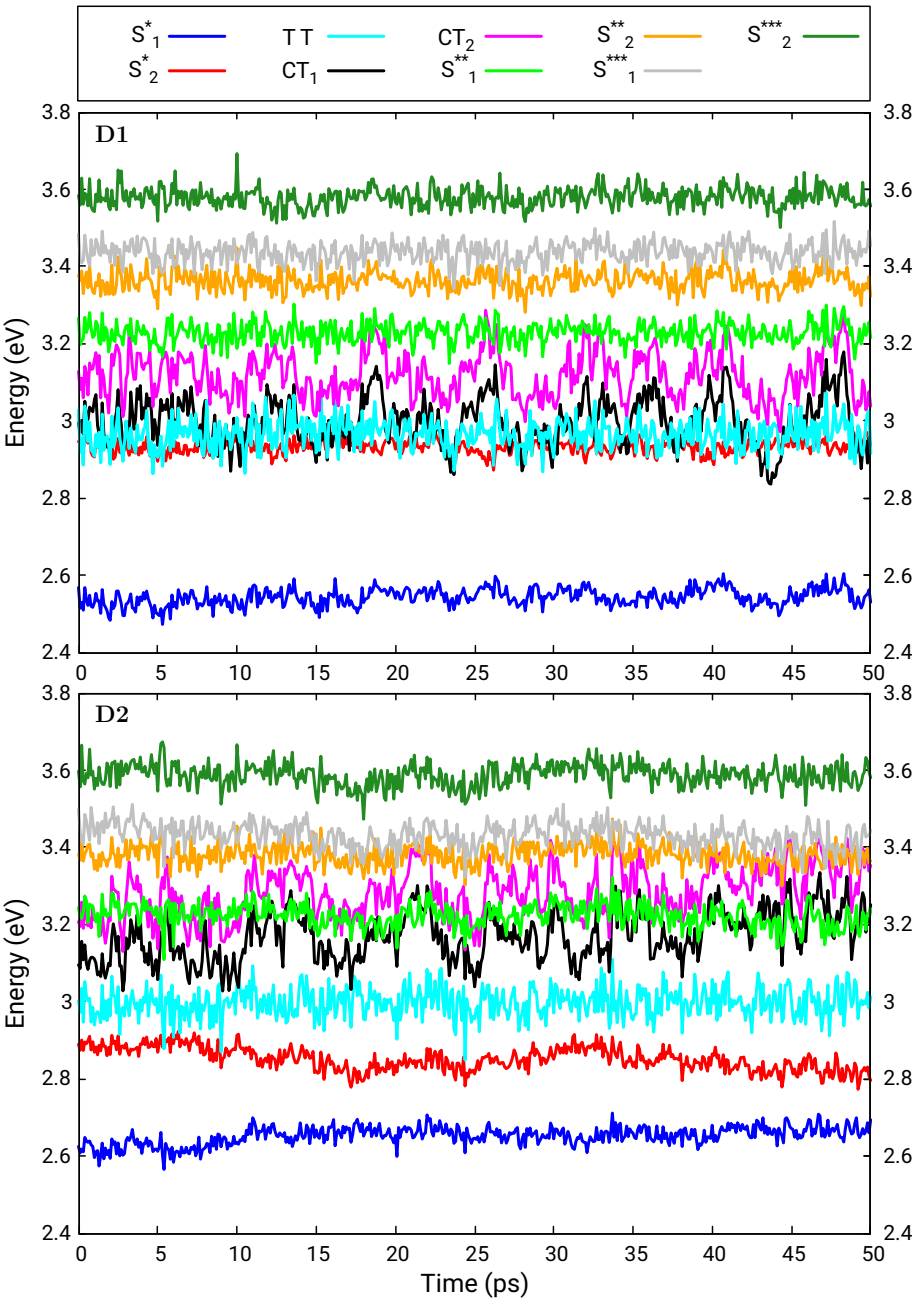


Figure S1: Excitation energies (in eV) from the ground state ($S_0S_0$) in the excitonic representation, obtained from the ground state thermal equilibrations for dimers **D1** (upper panel) and **D2** (lower panel) of ML-DPBF. Each point in the plot is obtained by averaging over a time interval of 100 fs.

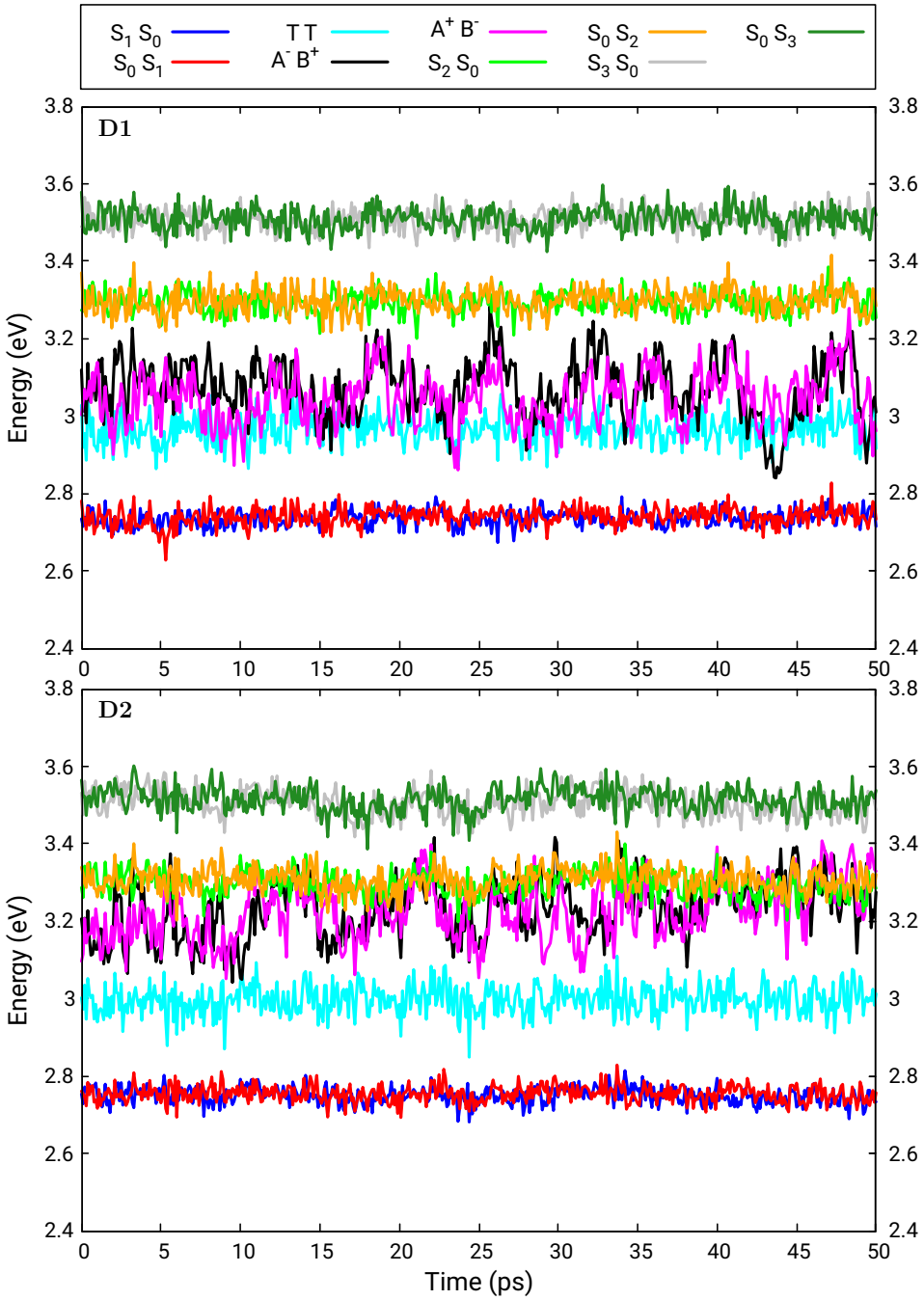


Figure S2: Excitation energies (in eV) from the ground state ($S_0S_0$) in the diabatic representation, obtained from the ground state thermal equilibrations for dimers **D1** (upper panel) and **D2** (lower panel) of ML-DPBF. Each point in the plot is obtained by averaging over a time interval of 100 fs.

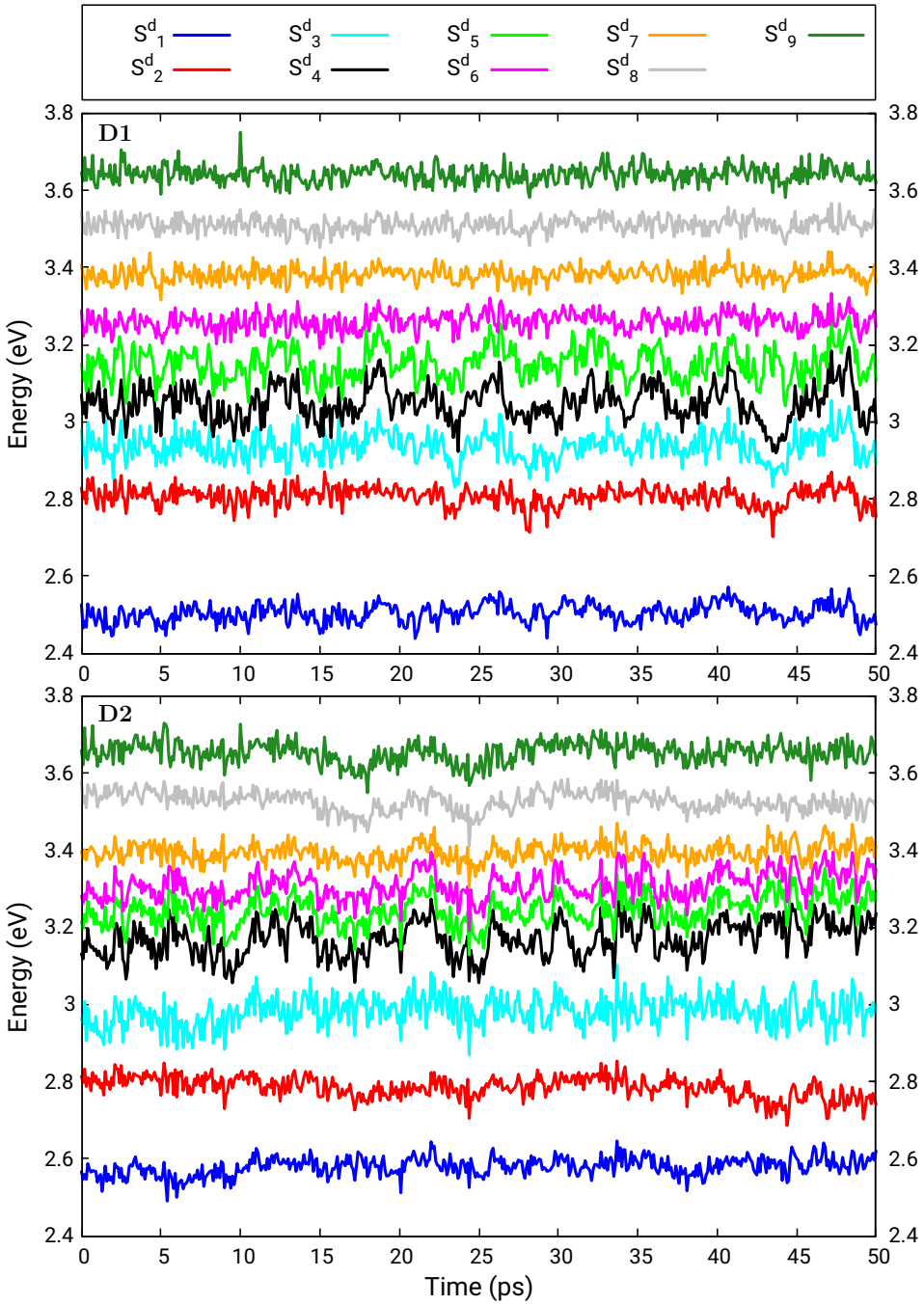


Figure S3: Excitation energies (in eV) from the ground state ($S_0^d$) in the adiabatic representation, obtained from the ground state thermal equilibrations for dimers **D1** (upper panel) and **D2** (lower panel) of ML-DPBF. A superscript $d$ is added to the state labels to indicate that they are the adiabatic states of the dimers. Each point in the plot is obtained by averaging over a time interval of 100 fs.

Table S2: Average values (diagonal and lower triangular part) and standard deviations (upper triangular part) of the electronic Hamiltonian matrix elements for the excitonic basis obtained from the ground state thermal equilibration of dimers **D1** and **D2** of ML-DPBF. All matrix elements are in units of meV. Averaging time intervals: 20-50 ps (**D1**) and 12-50 ps (**D2**).

Dimer **D1**

| $\hat{\mathcal{H}}_{el}$ | $S_0S_0$ | $S_1^*$ | $S_2^*$ | $TT$ | $CT_1$ | $CT_2$ | $S_1^{**}$ | $S_2^{**}$ | $S_1^{***}$ | $S_2^{***}$ |
|---|---|---|---|---|---|---|---|---|---|---|
| $S_0S_0$ | 0.00 | ± 30.56 | ± 37.91 | ± 1.88 | ± 61.55 | ± 48.21 | ± 43.59 | ± 39.75 | ± 51.43 | ± 55.56 |
| $S_1^*$ | 2.09 | 2548.57 | ± 0.00 | ± 1.93 | ± 54.56 | ± 58.62 | ± 43.24 | ± 43.53 | ± 146.05 | ± 91.40 |
| $S_2^*$ | -62.09 | 0.00 | 2931.90 | ± 3.21 | ± 53.16 | ± 52.48 | ± 114.81 | ± 119.86 | ± 99.07 | ± 143.38 |
| $TT$ | 0.33 | 0.49 | -1.91 | 2965.12 | ± 46.55 | ± 52.85 | ± 2.43 | ± 2.68 | ± 1.72 | ± 2.27 |
| $CT_1$ | 1.35 | -11.51 | 6.67 | 4.52 | 2998.97 | ± 0.00 | ± 16.42 | ± 14.48 | ± 12.93 | ± 11.38 |
| $CT_2$ | -2.45 | -12.92 | 4.34 | 1.71 | 0.00 | 3118.27 | ± 13.19 | ± 14.25 | ± 10.11 | ± 11.61 |
| $S_1^{**}$ | -1.23 | -1.06 | -3.60 | 0.00 | 1.20 | 0.15 | 3230.15 | ± 0.00 | ± 32.98 | ± 16.39 |
| $S_2^{**}$ | -1.22 | -0.97 | -3.87 | 0.02 | 0.92 | -0.06 | 0.00 | 3363.82 | ± 20.76 | ± 26.02 |
| $S_1^{***}$ | -1.76 | 11.50 | 2.84 | 0.00 | 0.28 | 0.00 | 0.10 | -0.39 | 3437.81 | ± 0.00 |
| $S_2^{***}$ | -2.65 | 3.72 | 6.87 | 0.01 | 0.02 | 0.04 | -0.21 | 0.47 | 0.00 | 3580.06 |

Dimer **D2**

| $\hat{\mathcal{H}}_{el}$ | $S_0S_0$ | $S_1^*$ | $S_2^*$ | $TT$ | $CT_1$ | $CT_2$ | $S_1^{**}$ | $S_2^{**}$ | $S_1^{***}$ | $S_2^{***}$ |
|---|---|---|---|---|---|---|---|---|---|---|
| $S_0S_0$ | 0.00 | ± 59.51 | ± 41.45 | ± 2.18 | ± 48.79 | ± 50.52 | ± 45.43 | ± 20.88 | ± 30.04 | ± 36.31 |
| $S_1^*$ | 58.73 | 2659.50 | ± 0.00 | ± 2.89 | ± 72.21 | ± 76.18 | ± 113.44 | ± 87.98 | ± 127.91 | ± 135.07 |
| $S_2^*$ | -0.69 | 0.00 | 2841.85 | ± 1.44 | ± 45.79 | ± 44.99 | ± 69.86 | ± 76.23 | ± 116.02 | ± 114.30 |
| $TT$ | 2.12 | 0.58 | 0.01 | 2999.14 | ± 43.79 | ± 43.47 | ± 4.24 | ± 2.82 | ± 2.71 | ± 3.28 |
| $CT_1$ | -1.56 | 3.68 | -7.20 | 0.65 | 3183.39 | ± 0.00 | ± 29.28 | ± 23.27 | ± 39.88 | ± 32.35 |
| $CT_2$ | 6.70 | -1.81 | -6.72 | 5.33 | 0.00 | 3298.34 | ± 25.36 | ± 25.45 | ± 31.45 | ± 40.87 |
| $S_1^{**}$ | -0.26 | -3.70 | 0.02 | 0.47 | 2.64 | 0.04 | 3219.38 | ± 0.00 | ± 28.26 | ± 29.72 |
| $S_2^{**}$ | 0.29 | -0.72 | 3.09 | 0.19 | 1.06 | 0.43 | 0.00 | 3381.45 | ± 22.98 | ± 22.11 |
| $S_1^{***}$ | -1.05 | -1.41 | -4.56 | 0.05 | -0.25 | -0.80 | 0.53 | -0.19 | 3427.24 | ± 0.00 |
| $S_2^{***}$ | -1.77 | -9.41 | -1.92 | -0.10 | 1.11 | 1.00 | -2.06 | -0.14 | 0.00 | 3585.42 |

Table S3: Average values (diagonal and lower triangular part) and standard deviations (upper triangular part) of the electronic Hamiltonian matrix elements for the diabatic basis obtained from the ground state thermal equilibration of dimers **D1** and **D2** of ML-DPBF. All matrix elements are in units of meV. Averaging time intervals: 20-50 ps (**D1**) and 12-50 ps (**D2**).

Dimer **D1**

| $\hat{\mathcal{H}}_{el}$ | $S_0S_0$ | $S_1S_0$ | $S_0S_1$ | $TT$ | $A^-B^+$ | $A^+B^-$ | $S_2S_0$ | $S_0S_2$ | $S_3S_0$ | $S_0S_3$ |
|---|---|---|---|---|---|---|---|---|---|---|
| $S_0S_0$ | 0.00 | ± 33.43 | ± 33.42 | ± 1.88 | ± 46.81 | ± 44.31 | ± 42.42 | ± 40.59 | ± 54.57 | ± 48.62 |
| $S_1S_0$ | -45.78 | 2737.57 | ± 20.02 | ± 2.83 | ± 23.37 | ± 23.96 | ± 83.35 | ± 95.02 | ± 172.95 | ± 26.83 |
| $S_0S_1$ | -43.60 | 183.95 | 2742.90 | ± 2.42 | ± 24.20 | ± 24.10 | ± 89.99 | ± 82.88 | ± 25.04 | ± 153.91 |
| $TT$ | 0.33 | -1.72 | -1.02 | 2965.12 | ± 38.66 | ± 41.65 | ± 2.51 | ± 2.59 | ± 2.08 | ± 1.84 |
| $A^-B^+$ | -21.17 | -71.26 | -0.41 | -34.97 | 3068.08 | ± 0.81 | ± 6.00 | ± 18.06 | ± 3.39 | ± 15.71 |
| $A^+B^-$ | -38.95 | 0.24 | -70.65 | -23.07 | -0.57 | 3049.16 | ± 21.12 | ± 6.40 | ± 15.85 | ± 3.90 |
| $S_2S_0$ | 4.49 | 8.13 | 13.23 | 0.31 | -0.84 | 2.71 | 3294.57 | ± 12.98 | ± 32.82 | ± 13.11 |
| $S_0S_2$ | -4.06 | -9.22 | -8.40 | 0.03 | 1.08 | -0.31 | 0.53 | 3299.39 | ± 11.83 | ± 32.68 |
| $S_3S_0$ | -2.18 | 6.54 | -0.21 | -0.15 | 0.19 | -2.60 | -1.72 | -0.35 | 3507.97 | ± 11.96 |
| $S_0S_3$ | 19.90 | -1.42 | -72.55 | -0.62 | 1.21 | -0.88 | 0.23 | 2.12 | 0.83 | 3509.90 |

Dimer **D2**

| $\hat{\mathcal{H}}_{el}$ | $S_0S_0$ | $S_1S_0$ | $S_0S_1$ | $TT$ | $A^-B^+$ | $A^+B^-$ | $S_2S_0$ | $S_0S_2$ | $S_3S_0$ | $S_0S_3$ |
|---|---|---|---|---|---|---|---|---|---|---|
| $S_0S_0$ | 0.00 | ± 34.17 | ± 35.14 | ± 2.18 | ± 47.51 | ± 47.40 | ± 35.03 | ± 35.49 | ± 30.79 | ± 35.72 |
| $S_1S_0$ | 53.44 | 2748.00 | ± 23.83 | ± 1.87 | ± 46.24 | ± 29.70 | ± 56.80 | ± 112.63 | ± 171.94 | ± 32.32 |
| $S_0S_1$ | 58.74 | -73.21 | 2753.35 | ± 2.28 | ± 28.55 | ± 43.59 | ± 110.37 | ± 55.27 | ± 31.13 | ± 169.45 |
| $TT$ | 2.12 | 0.92 | 1.10 | 2999.14 | ± 42.63 | ± 41.90 | ± 3.56 | ± 3.65 | ± 3.04 | ± 2.96 |
| $A^-B^+$ | -14.79 | 53.10 | 45.45 | -12.14 | 3246.69 | ± 0.93 | ± 7.91 | ± 39.28 | ± 3.84 | ± 50.18 |
| $A^+B^-$ | -16.07 | 45.56 | 50.55 | -10.80 | 0.57 | 3235.04 | ± 31.72 | ± 7.73 | ± 51.55 | ± 3.77 |
| $S_2S_0$ | 1.14 | 1.28 | 5.35 | 0.06 | -0.25 | -2.33 | 3294.68 | ± 33.20 | ± 26.69 | ± 26.45 |
| $S_0S_2$ | -3.41 | -11.93 | -1.36 | 0.48 | 4.50 | 0.87 | -12.97 | 3306.15 | ± 24.23 | ± 26.24 |
| $S_3S_0$ | -0.87 | -10.25 | -1.02 | 0.23 | 0.04 | 3.67 | -0.96 | 3.80 | 3500.16 | ± 25.17 |
| $S_0S_3$ | 0.39 | -1.79 | -29.05 | -0.33 | -9.02 | -0.15 | -0.14 | 0.91 | -0.58 | 3512.49 |

Table S4: Average values (diagonal and lower triangular part) and standard deviations (upper triangular part) of the effective electronic Hamiltonian matrix in both the excitonic basis and the diabatic one obtained from the ground state thermal equilibrations of dimers **D1** and **D2** of ML-DPBF. In the construction of the effective Hamiltonian matrix (see Section S1.2 for more details), the outer space is spanned by either the excitonic states $CT_1$, $CT_2$, $S_1^{**}$ and $S_2^{**}$, or the diabatic states $A^-B^+$, $A^+B^-$, $S_2S_0$ and $S_0S_2$. All matrix elements are in units of meV. Averaging time intervals: 20-50 ps (**D1**) and 12-50 ps (**D2**).

Dimer **D1**

| $\hat{\mathcal{H}}_{el}^{eff}$ | $S_1^*$ | $S_2^*$ | $TT$ |
|---|---|---|---|
| $S_1^*$ | 2531.32 | $\pm$ 14.02 | $\pm$ 14.30 |
| $S_2^*$ | 0.33 | 2846.42 | $\pm$ 27.59 |
| $TT$ | -0.49 | 0.64 | 2946.37 |

| $\hat{\mathcal{H}}_{el}^{eff}$ | $S_1S_0$ | $S_0S_1$ | $TT$ |
|---|---|---|---|
| $S_1S_0$ | 2686.06 | $\pm$ 24.72 | $\pm$ 23.03 |
| $S_0S_1$ | 149.40 | 2691.68 | $\pm$ 20.85 |
| $TT$ | -1.11 | -0.58 | 2946.37 |

Dimer **D2**

| $\hat{\mathcal{H}}_{el}^{eff}$ | $S_1^*$ | $S_2^*$ | $TT$ |
|---|---|---|---|
| $S_1^*$ | 2609.99 | $\pm$ 15.94 | $\pm$ 20.89 |
| $S_2^*$ | -0.19 | 2809.06 | $\pm$ 11.38 |
| $TT$ | -2.86 | -0.17 | 2984.83 |

| $\hat{\mathcal{H}}_{el}^{eff}$ | $S_1S_0$ | $S_0S_1$ | $TT$ |
|---|---|---|---|
| $S_1S_0$ | 2705.70 | $\pm$ 48.59 | $\pm$ 17.25 |
| $S_0S_1$ | -77.28 | 2713.35 | $\pm$ 16.54 |
| $TT$ | -1.53 | 0.63 | 2984.83 |

Table S5: Average weights (square coefficients) of the excitonic states in the 10 low-lying adiabatic states obtained in the thermal equilibrations on $S_0^d$ for dimers **D1** and **D2** of ML-DPBF. Weights > 0.1 are in bold. The relative energies (in eV) of the adiabatic states and the transition dipole moments squared (a.u.) for the adiabatic and the excitonic states are also reported. Averaging time intervals: 20-50 ps (**D1**) and 12-50 ps (**D2**).

Dimer **D1**

| | $S_0S_0$ | $S_1^*$ | $S_2^*$ | $TT$ | $CT_1$ | $CT_2$ | $S_1^{**}$ | $S_2^{**}$ | $S_1^{***}$ | $S_2^{***}$ | Energy (eV) | $\mu^2_{S_0^d \to S_n^d}$ (a.u.) |
|---|---|---|---|---|---|---|---|---|---|---|---|---|
| $S_0^d$ | **0.998** | 0.000 | 0.001 | 0.000 | 0.000 | 0.000 | 0.000 | 0.000 | 0.000 | 0.000 | 0.000 | - |
| $S_1^d$ | 0.000 | **0.939** | 0.001 | 0.001 | 0.013 | 0.009 | 0.004 | 0.003 | 0.024 | 0.007 | 2.507 | 4.247 |
| $S_2^d$ | 0.001 | 0.003 | **0.623** | **0.148** | 0.090 | 0.033 | 0.041 | 0.027 | 0.013 | 0.022 | 2.803 | 15.260 |
| $S_3^d$ | 0.000 | 0.004 | **0.170** | **0.501** | **0.244** | 0.034 | 0.023 | 0.010 | 0.005 | 0.008 | 2.934 | 4.253 |
| $S_4^d$ | 0.000 | 0.010 | 0.025 | **0.186** | **0.577** | **0.166** | 0.025 | 0.005 | 0.003 | 0.002 | 3.048 | 0.645 |
| $S_5^d$ | 0.000 | 0.005 | 0.016 | **0.141** | 0.058 | **0.633** | **0.124** | 0.010 | 0.010 | 0.002 | 3.154 | 0.847 |
| $S_6^d$ | 0.000 | 0.005 | 0.032 | 0.022 | 0.011 | **0.111** | **0.668** | 0.091 | 0.052 | 0.008 | 3.264 | 4.193 |
| $S_7^d$ | 0.000 | 0.005 | 0.033 | 0.001 | 0.003 | 0.011 | 0.070 | **0.668** | **0.162** | 0.046 | 3.382 | 3.165 |
| $S_8^d$ | 0.000 | 0.024 | 0.034 | 0.000 | 0.001 | 0.002 | 0.034 | **0.143** | **0.700** | 0.061 | 3.512 | 1.180 |
| $S_9^d$ | 0.000 | 0.004 | 0.068 | 0.000 | 0.001 | 0.001 | 0.011 | 0.041 | 0.030 | **0.844** | 3.641 | 0.792 |
| $\mu^2_{0 \to i(exc.)}$ (a.u.) | - | 4.092 | 13.887 | 1.727 | 2.182 | 1.134 | 4.718 | 3.806 | 1.525 | 1.420 | - | - |

Dimer **D2**

| | $S_0S_0$ | $S_1^*$ | $S_2^*$ | $TT$ | $CT_1$ | $CT_2$ | $S_1^{**}$ | $S_2^{**}$ | $S_1^{***}$ | $S_2^{***}$ | Energy (eV) | $\mu^2_{S_0^d \to S_n^d}$ (a.u.) |
|---|---|---|---|---|---|---|---|---|---|---|---|---|
| $S_0^d$ | **0.998** | 0.001 | 0.000 | 0.000 | 0.000 | 0.000 | 0.000 | 0.000 | 0.000 | 0.000 | 0.000 | - |
| $S_1^d$ | 0.001 | **0.895** | 0.003 | 0.002 | 0.014 | 0.011 | 0.029 | 0.011 | 0.019 | 0.015 | 2.584 | 2.531 |
| $S_2^d$ | 0.000 | 0.006 | **0.845** | 0.050 | 0.012 | 0.006 | 0.024 | 0.014 | 0.028 | 0.015 | 2.779 | 25.193 |
| $S_3^d$ | 0.000 | 0.005 | 0.049 | **0.810** | 0.094 | 0.018 | 0.015 | 0.002 | 0.005 | 0.003 | 2.988 | 1.477 |
| $S_4^d$ | 0.000 | 0.012 | 0.018 | 0.077 | **0.506** | 0.046 | **0.288** | 0.009 | 0.027 | 0.017 | 3.176 | 0.692 |
| $S_5^d$ | 0.000 | 0.011 | 0.013 | 0.035 | **0.264** | **0.243** | **0.339** | 0.036 | 0.035 | 0.023 | 3.248 | 0.708 |
| $S_6^d$ | 0.000 | 0.007 | 0.008 | 0.016 | 0.063 | **0.417** | **0.249** | **0.156** | 0.067 | 0.017 | 3.314 | 0.892 |
| $S_7^d$ | 0.000 | 0.008 | 0.008 | 0.008 | 0.024 | **0.194** | 0.023 | **0.547** | **0.171** | 0.018 | 3.395 | 1.702 |
| $S_8^d$ | 0.000 | 0.026 | 0.034 | 0.001 | 0.014 | 0.039 | 0.016 | **0.209** | **0.635** | 0.025 | 3.521 | 1.595 |
| $S_9^d$ | 0.000 | 0.030 | 0.021 | 0.000 | 0.009 | 0.026 | 0.017 | 0.017 | 0.012 | **0.867** | 3.651 | 0.389 |
| $\mu^2_{0 \to i(exc.)}$ (a.u.) | - | 2.489 | 23.650 | 0.322 | 0.809 | 0.738 | 1.677 | 2.539 | 2.021 | 0.883 | - | - |

Table S6: Average weights (square coefficients) of the diabatic states in the 10 low-lying adiabatic states obtained in the thermal equilibrations on $S_0^d$ for dimers **D1** and **D2** of ML-DPBF. Weights > 0.1 are in bold. The relative energies (in eV) of the adiabatic states and the transition dipole moments squared (a.u.) for the adiabatic and the diabatic states are also reported. Averaging time intervals: 20-50 ps (**D1**) and 12-50 ps (**D2**).

Dimer **D1**

| | $S_0S_0$ | $S_1S_0$ | $S_0S_1$ | $TT$ | $A^-B^+$ | $A^+B^-$ | $S_2S_0$ | $S_0S_2$ | $S_3S_0$ | $S_0S_3$ | Energy (eV) | $\mu^2_{S_0^d \to S_n^d}$ (a.u.) |
|---|---|---|---|---|---|---|---|---|---|---|---|---|
| $S_0^d$ | **0.998** | 0.000 | 0.000 | 0.000 | 0.000 | 0.000 | 0.000 | 0.000 | 0.000 | 0.000 | 0.000 | - |
| $S_1^d$ | 0.000 | **0.480** | **0.460** | 0.001 | 0.011 | 0.011 | 0.003 | 0.003 | 0.015 | 0.016 | 2.507 | 4.247 |
| $S_2^d$ | 0.001 | **0.303** | **0.323** | **0.148** | 0.062 | 0.061 | 0.033 | 0.034 | 0.018 | 0.017 | 2.803 | 15.260 |
| $S_3^d$ | 0.000 | 0.086 | 0.087 | **0.501** | **0.128** | **0.150** | 0.017 | 0.017 | 0.007 | 0.006 | 2.934 | 4.253 |
| $S_4^d$ | 0.000 | 0.017 | 0.018 | **0.186** | **0.328** | **0.415** | 0.017 | 0.013 | 0.003 | 0.003 | 3.048 | 0.645 |
| $S_5^d$ | 0.000 | 0.011 | 0.010 | **0.141** | **0.386** | **0.305** | 0.071 | 0.063 | 0.007 | 0.005 | 3.154 | 0.847 |
| $S_6^d$ | 0.000 | 0.018 | 0.018 | 0.022 | 0.074 | 0.048 | **0.386** | **0.373** | 0.030 | 0.030 | 3.264 | 4.193 |
| $S_7^d$ | 0.000 | 0.019 | 0.019 | 0.001 | 0.008 | 0.006 | **0.360** | **0.378** | **0.109** | **0.100** | 3.382 | 3.165 |
| $S_8^d$ | 0.000 | 0.030 | 0.028 | 0.000 | 0.002 | 0.002 | 0.087 | 0.091 | **0.372** | **0.389** | 3.512 | 1.180 |
| $S_9^d$ | 0.000 | 0.036 | 0.036 | 0.000 | 0.001 | 0.001 | 0.025 | 0.027 | **0.439** | **0.434** | 3.641 | 0.792 |
| $\mu^2_{0\to i(dia.)}$ (a.u.) | - | 8.878 | 9.101 | 1.727 | 1.649 | 1.667 | 4.252 | 4.272 | 1.519 | 1.426 | - | - |

Dimer **D2**

| | $S_0S_0$ | $S_1S_0$ | $S_0S_1$ | $TT$ | $A^-B^+$ | $A^+B^-$ | $S_2S_0$ | $S_0S_2$ | $S_3S_0$ | $S_0S_3$ | Energy (eV) | $\mu^2_{S_0^d \to S_n^d}$ (a.u.) |
|---|---|---|---|---|---|---|---|---|---|---|---|---|
| $S_0^d$ | **0.998** | 0.001 | 0.001 | 0.000 | 0.000 | 0.000 | 0.000 | 0.000 | 0.000 | 0.000 | 0.000 | - |
| $S_1^d$ | 0.001 | **0.466** | **0.432** | 0.002 | 0.013 | 0.012 | 0.020 | 0.020 | 0.018 | 0.017 | 2.584 | 2.531 |
| $S_2^d$ | 0.000 | **0.409** | **0.443** | 0.050 | 0.009 | 0.010 | 0.018 | 0.019 | 0.021 | 0.022 | 2.779 | 25.193 |
| $S_3^d$ | 0.000 | 0.025 | 0.028 | **0.810** | 0.052 | 0.060 | 0.009 | 0.008 | 0.004 | 0.004 | 2.988 | 1.477 |
| $S_4^d$ | 0.000 | 0.016 | 0.014 | 0.077 | **0.252** | **0.300** | **0.160** | **0.137** | 0.023 | 0.021 | 3.176 | 0.692 |
| $S_5^d$ | 0.000 | 0.012 | 0.012 | 0.035 | **0.256** | **0.251** | **0.196** | **0.179** | 0.030 | 0.027 | 3.248 | 0.708 |
| $S_6^d$ | 0.000 | 0.007 | 0.007 | 0.016 | **0.254** | **0.225** | **0.208** | **0.198** | 0.045 | 0.039 | 3.314 | 0.892 |
| $S_7^d$ | 0.000 | 0.008 | 0.007 | 0.008 | **0.119** | 0.099 | **0.269** | **0.301** | 0.098 | 0.091 | 3.395 | 1.702 |
| $S_8^d$ | 0.000 | 0.032 | 0.029 | 0.001 | 0.027 | 0.027 | **0.102** | **0.122** | **0.347** | **0.313** | 3.521 | 1.595 |
| $S_9^d$ | 0.000 | 0.024 | 0.027 | 0.000 | 0.018 | 0.017 | 0.018 | 0.016 | **0.413** | **0.466** | 3.651 | 0.389 |
| $\mu^2_{0\to i(dia.)}$ (a.u.) | - | 12.732 | 13.407 | 0.322 | 0.803 | 0.745 | 2.076 | 2.140 | 1.455 | 1.449 | - | - |

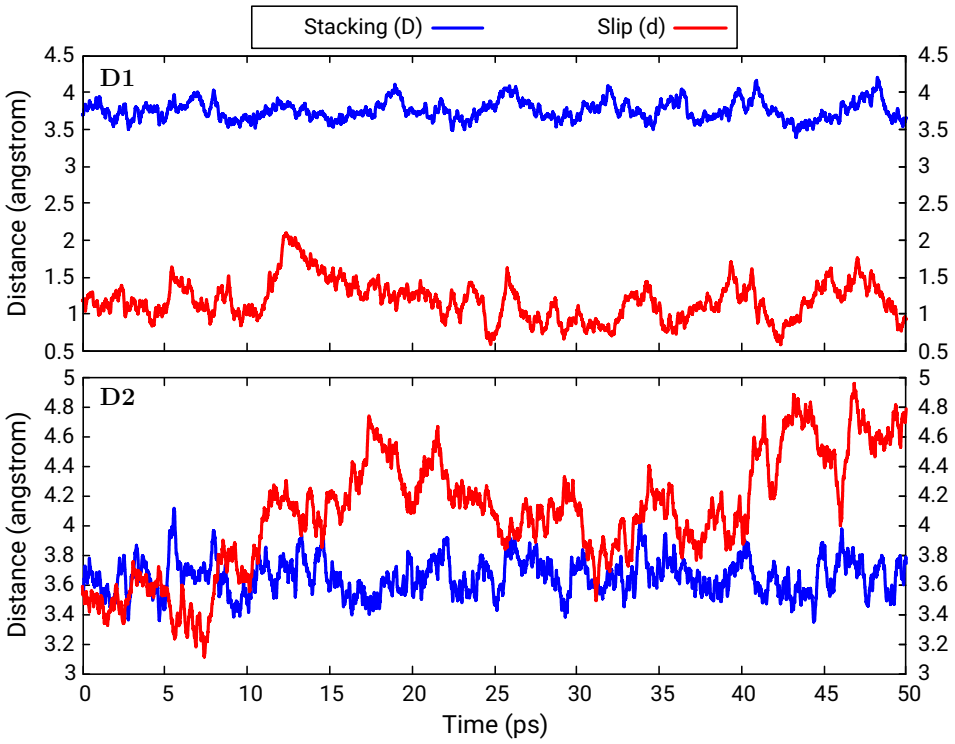


Figure S4: Stacking and slip distances (in Å) between chromophores obtained from the ground state thermal equilibrations for dimers **D1** (upper panel) and **D2** (lower panel) of ML-DPBF. The stacking distance ($D$) between chromophores is computed as the average distance beween the centroid of one chromophore and its projection to the best-fit plane of the other chromophore, while the slip distance ($d$) is defined as the average distance beween the centroid of one chromophore and the projection of the centroid of the other chromophore to the best-fit plane of the first chromophore.

## S2.2 Simulations of excited state dynamics

Table S7: Excitonic state populations at the starting geometries ($t = 0$) of the excited state dynamics for dimers **D1** and **D2** of ML-DPBF.

| State | Dimer **D1** | Dimer **D2** |
|---|---|---|
| $S_0S_0$ | 0.0006 | 0.0002 |
| $S_1^*$ | 0.0297 | 0.0578 |
| $S_2^*$ | 0.6702 | 0.8263 |
| $TT$ | 0.0746 | 0.0122 |
| $CT_1$ | 0.0799 | 0.0139 |
| $CT_2$ | 0.0281 | 0.0073 |
| $S_1^{**}$ | 0.0464 | 0.0220 |
| $S_2^{**}$ | 0.0305 | 0.0143 |
| $S_1^{***}$ | 0.0154 | 0.0307 |
| $S_2^{***}$ | 0.0248 | 0.0154 |

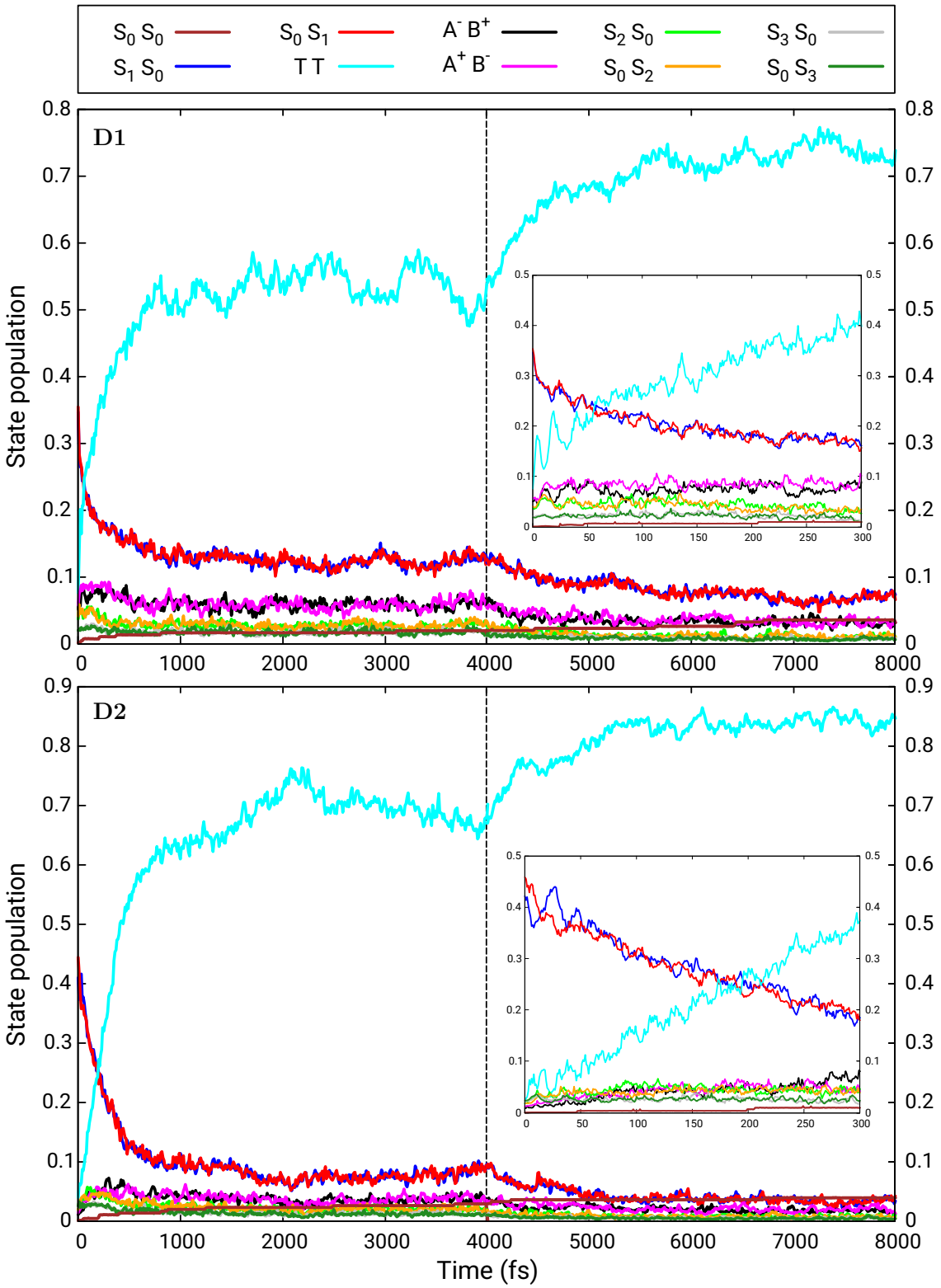


Figure S5: Diabatic state populations as functions of time for dimers **D1** (upper panels) and **D2** (lower panels) of ML-DPBF. In the first 4 ps the trajectories where propagated in constant energy mode, while in the time interval of 4-8 ps the van Gunsteren-Berendsen thermostat [23] was applied, with a temperature of 300 K. The reported results are obtained by averaging over all trajectories and time intervals of 10 fs (larger panels, 0-8000 fs) and 1 fs (smaller panels, 0-300 fs).

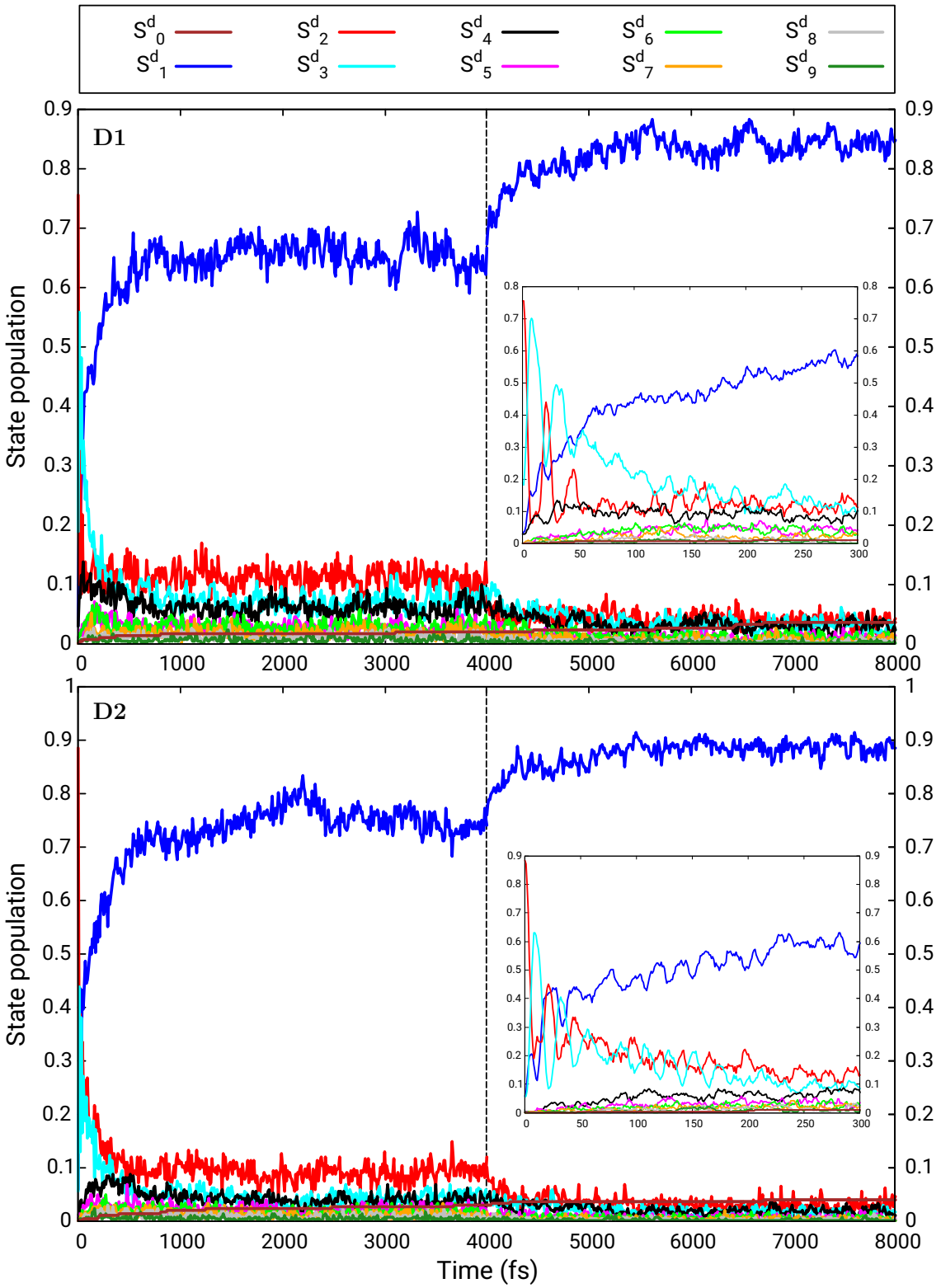


Figure S6: Adiabatic state populations as functions of time for dimers **D1** (upper panels) and **D2** (lower panels) of ML-DPBF. In the first 4 ps the trajectories where propagated in constant energy mode, while in the time interval of 4-8 ps the van Gunsteren-Berendsen thermostat [23] was applied, with a temperature of 300 K. A superscript $d$ is added to the state labels to indicate that they are the adiabatic states of the dimers. The reported results are obtained by averaging over all trajectories and time intervals of 10 fs (larger panels, 0-8000 fs) and 1 fs (smaller panels, 0-300 fs).

Table S8: Average transition rates between pairs of excitonic states obtained in the simulations of the excited state dynamics for dimers **D1** and **D2** of ML-DPBF. The $CT_n$ states, the higher excitonic states $S_1^{**}$ and $S_2^{**}$, and $S_1^{***}$ and $S_2^{***}$ are grouped together and indicated as $CT$, $S^{**}$ and $S^{***}$, respectively. Each rate, defined as $\frac{\#\ transitions}{\#\ trajectories\ \cdot\ time\ interval}$, is computed over the first 4 ps of the simulations and reported in units of ps$^{-1}$.

| States | | Dimer **D1** Rates (ps$^{-1}$) | | | Dimer **D2** Rates (ps$^{-1}$) | | |
|---|---|---|---|---|---|---|---|
| $i$ | $j$ | $i \to j$ | $j \to i$ | net[a] | $i \to j$ | $j \to i$ | net[a] |
| $S_1^*$ | $S_0S_0$ | 0.002 | 0.000 | 0.002 | 0.001 | 0.000 | 0.001 |
| $S_2^*$ | $S_0S_0$ | 0.001 | 0.000 | 0.001 | 0.003 | 0.000 | 0.003 |
| $TT$ | $S_0S_0$ | 0.001 | 0.000 | 0.001 | 0.001 | 0.000 | 0.001 |
| $CT$ | $S_0S_0$ | 0.000 | 0.000 | 0.000 | 0.000 | 0.000 | 0.000 |
| $S^{**}$ | $S_0S_0$ | 0.001 | 0.000 | 0.001 | 0.002 | 0.000 | 0.002 |
| $S^{***}$ | $S_0S_0$ | 0.000 | 0.000 | 0.000 | 0.001 | 0.001 | 0.000 |
| $S_2^*$ | $S_1^*$ | 0.957 | 1.199 | -0.242 | 1.477 | 1.459 | 0.018 |
| $TT$ | $S_1^*$ | 13.552 | 12.805 | 0.747 | 12.390 | 11.953 | 0.437 |
| $CT$ | $S_1^*$ | 0.444 | 0.555 | -0.111 | 0.189 | 0.262 | -0.073 |
| $S^{**}$ | $S_1^*$ | 0.182 | 0.404 | -0.222 | 0.143 | 0.388 | -0.245 |
| $S^{***}$ | $S_1^*$ | 0.034 | 0.160 | -0.126 | 0.033 | 0.149 | -0.116 |
| $TT$ | $S_2^*$ | 3.857 | 4.400 | -0.543 | 3.590 | 4.174 | -0.584 |
| $CT$ | $S_2^*$ | 5.883 | 5.630 | 0.253 | 1.934 | 1.477 | 0.457 |
| $S^{**}$ | $S_2^*$ | 1.162 | 1.242 | -0.080 | 0.710 | 0.740 | -0.030 |
| $S^{***}$ | $S_2^*$ | 0.238 | 0.314 | -0.076 | 0.105 | 0.149 | -0.044 |
| $CT$ | $TT$ | 3.104 | 2.783 | 0.321 | 0.991 | 0.913 | 0.078 |
| $S^{**}$ | $TT$ | 0.357 | 0.325 | 0.032 | 0.229 | 0.243 | -0.014 |
| $S^{***}$ | $TT$ | 0.046 | 0.066 | -0.020 | 0.027 | 0.061 | -0.034 |
| $S^{**}$ | $CT$ | 3.829 | 3.314 | 0.515 | 4.405 | 3.922 | 0.483 |
| $S^{***}$ | $CT$ | 0.567 | 0.606 | -0.039 | 0.598 | 0.609 | -0.011 |
| $S^{***}$ | $S^{**}$ | 3.347 | 3.089 | 0.258 | 2.289 | 2.088 | 0.201 |

[a] Difference between the $i \to j$ rate and the $j \to i$ one.

Table S9: Average transition rates between pairs of excitonic states obtained in the simulations of the excited state dynamics for dimers **D1** and **D2** of ML-DPBF. Each rate, defined as $\frac{\#\ transitions}{\#\ trajectories\ \cdot\ time\ interval}$, is computed over the first 4 ps of the simulations and reported in units of $ps^{-1}$.

| States | | Dimer **D1** Rates ($ps^{-1}$) | | | Dimer **D2** Rates ($ps^{-1}$) | | |
|---|---|---|---|---|---|---|---|
| $i$ | $j$ | $i \rightarrow j$ | $j \rightarrow i$ | net[a] | $i \rightarrow j$ | $j \rightarrow i$ | net[a] |
| $S_1^*$ | $S_0S_0$ | 0.002 | 0.000 | 0.002 | 0.001 | 0.000 | 0.001 |
| $S_2^*$ | $S_0S_0$ | 0.001 | 0.000 | 0.001 | 0.003 | 0.000 | 0.003 |
| $TT$ | $S_0S_0$ | 0.001 | 0.000 | 0.001 | 0.001 | 0.000 | 0.001 |
| $CT_1$ | $S_0S_0$ | 0.000 | 0.000 | 0.000 | 0.000 | 0.000 | 0.000 |
| $CT_2$ | $S_0S_0$ | 0.000 | 0.000 | 0.000 | 0.000 | 0.000 | 0.000 |
| $S_1^{**}$ | $S_0S_0$ | 0.000 | 0.000 | 0.000 | 0.002 | 0.000 | 0.002 |
| $S_2^{**}$ | $S_0S_0$ | 0.001 | 0.000 | 0.001 | 0.000 | 0.000 | 0.000 |
| $S_1^{***}$ | $S_0S_0$ | 0.000 | 0.000 | 0.000 | 0.000 | 0.001 | -0.001 |
| $S_2^{***}$ | $S_0S_0$ | 0.000 | 0.000 | 0.000 | 0.001 | 0.000 | 0.001 |
| $S_2^*$ | $S_1^*$ | 0.957 | 1.199 | -0.242 | 1.477 | 1.459 | 0.018 |
| $TT$ | $S_1^*$ | 13.552 | 12.805 | 0.747 | 12.390 | 11.953 | 0.437 |
| $CT_1$ | $S_1^*$ | 0.382 | 0.388 | -0.006 | 0.147 | 0.156 | -0.009 |
| $CT_2$ | $S_1^*$ | 0.062 | 0.167 | -0.105 | 0.042 | 0.106 | -0.064 |
| $S_1^{**}$ | $S_1^*$ | 0.131 | 0.256 | -0.125 | 0.102 | 0.265 | -0.163 |
| $S_2^{**}$ | $S_1^*$ | 0.050 | 0.147 | -0.097 | 0.041 | 0.123 | -0.082 |
| $S_1^{***}$ | $S_1^*$ | 0.026 | 0.106 | -0.080 | 0.029 | 0.100 | -0.071 |
| $S_2^{***}$ | $S_1^*$ | 0.008 | 0.054 | -0.046 | 0.004 | 0.049 | -0.045 |
| $TT$ | $S_2^*$ | 3.857 | 4.400 | -0.543 | 3.590 | 4.174 | -0.584 |
| $CT_1$ | $S_2^*$ | 5.343 | 4.916 | 0.427 | 1.785 | 1.305 | 0.480 |
| $CT_2$ | $S_2^*$ | 0.540 | 0.714 | -0.174 | 0.149 | 0.173 | -0.024 |
| $S_1^{**}$ | $S_2^*$ | 1.104 | 1.100 | 0.004 | 0.662 | 0.634 | 0.028 |
| $S_2^{**}$ | $S_2^*$ | 0.057 | 0.143 | -0.086 | 0.048 | 0.106 | -0.058 |
| $S_1^{***}$ | $S_2^*$ | 0.219 | 0.256 | -0.037 | 0.096 | 0.115 | -0.019 |
| $S_2^{***}$ | $S_2^*$ | 0.019 | 0.057 | -0.038 | 0.010 | 0.034 | -0.024 |
| $CT_1$ | $TT$ | 2.769 | 2.304 | 0.465 | 0.869 | 0.695 | 0.174 |
| $CT_2$ | $TT$ | 0.335 | 0.479 | -0.144 | 0.122 | 0.218 | -0.096 |
| $S_1^{**}$ | $TT$ | 0.322 | 0.283 | 0.039 | 0.208 | 0.191 | 0.017 |
| $S_2^{**}$ | $TT$ | 0.035 | 0.042 | -0.007 | 0.021 | 0.051 | -0.030 |
| $S_1^{***}$ | $TT$ | 0.041 | 0.045 | -0.004 | 0.023 | 0.034 | -0.011 |
| $S_2^{***}$ | $TT$ | 0.006 | 0.021 | -0.015 | 0.004 | 0.027 | -0.023 |
| $CT_2$ | $CT_1$ | 4.037 | 3.027 | 1.010 | 2.263 | 1.617 | 0.646 |
| $S_1^{**}$ | $CT_1$ | 1.048 | 0.992 | 0.056 | 1.749 | 1.667 | 0.082 |
| $S_2^{**}$ | $CT_1$ | 0.037 | 0.116 | -0.079 | 0.068 | 0.104 | -0.036 |
| $S_1^{***}$ | $CT_1$ | 0.131 | 0.178 | -0.047 | 0.176 | 0.186 | -0.010 |
| $S_2^{***}$ | $CT_1$ | 0.009 | 0.054 | -0.045 | 0.013 | 0.041 | -0.028 |
| $S_1^{**}$ | $CT_2$ | 2.595 | 2.066 | 0.529 | 2.223 | 1.846 | 0.377 |
| $S_2^{**}$ | $CT_2$ | 0.150 | 0.139 | 0.011 | 0.366 | 0.305 | 0.061 |
| $S_1^{***}$ | $CT_2$ | 0.418 | 0.356 | 0.062 | 0.391 | 0.350 | 0.041 |
| $S_2^{***}$ | $CT_2$ | 0.009 | 0.018 | -0.009 | 0.018 | 0.031 | -0.013 |
| $S_2^{**}$ | $S_1^{**}$ | 1.885 | 1.491 | 0.394 | 1.071 | 0.803 | 0.268 |
| $S_1^{***}$ | $S_1^{**}$ | 1.230 | 1.111 | 0.119 | 0.678 | 0.600 | 0.078 |
| $S_2^{***}$ | $S_1^{**}$ | 0.100 | 0.100 | 0.000 | 0.057 | 0.055 | 0.002 |
| $S_1^{***}$ | $S_2^{**}$ | 1.632 | 1.510 | 0.122 | 1.303 | 1.198 | 0.105 |
| $S_2^{***}$ | $S_2^{**}$ | 0.385 | 0.369 | 0.016 | 0.252 | 0.235 | 0.017 |
| $S_2^{***}$ | $S_1^{***}$ | 0.623 | 0.486 | 0.137 | 0.416 | 0.303 | 0.113 |

[a] Difference between the $i \rightarrow j$ rate and the $j \rightarrow i$ one.

Figure S7: Net transition rates (in $ps^{-1}$) between pairs of states as functions of time (fs), obtained from the simulation of the excited state dynamics for dimer **D1** of ML-DPBF. The $CT_n$ states, the higher excitonic states $S_1^{**}$ and $S_2^{**}$, and $S_1^{***}$ and $S_2^{***}$ are grouped together and indicated as $CT$, $S^{**}$ and $S^{***}$, respectively. Each rate is defined as $\frac{\#\ transitions}{\#\ trajectories\ \cdot\ time\ interval}$. For each type of transition, one bar represents a net transition rate computed in a time interval of 25 fs (e.g. the first bar corresponds to the interval $(0{:}25]$ fs). For panels f-j, see the next page.

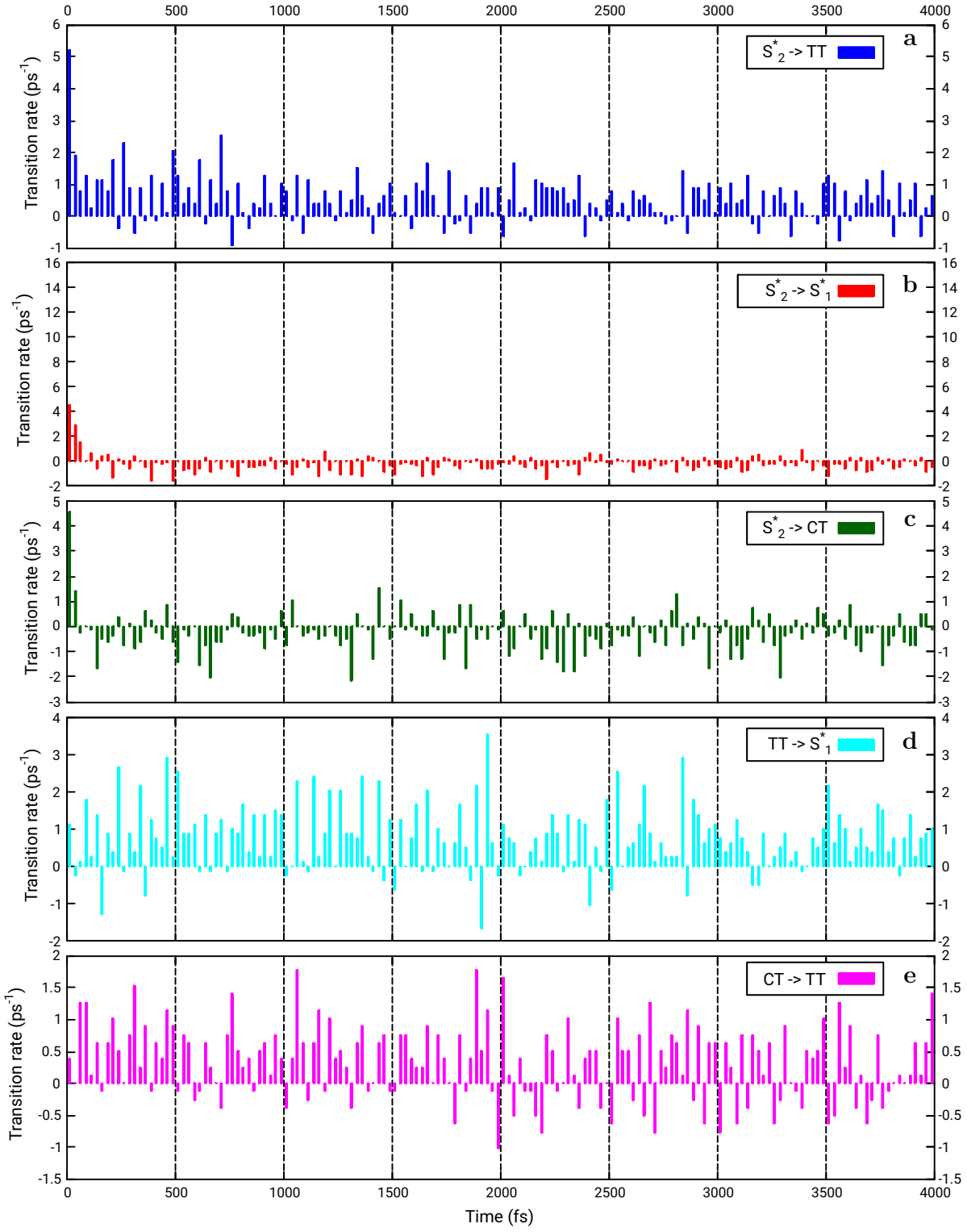

Figure S7: (continued from previous page)

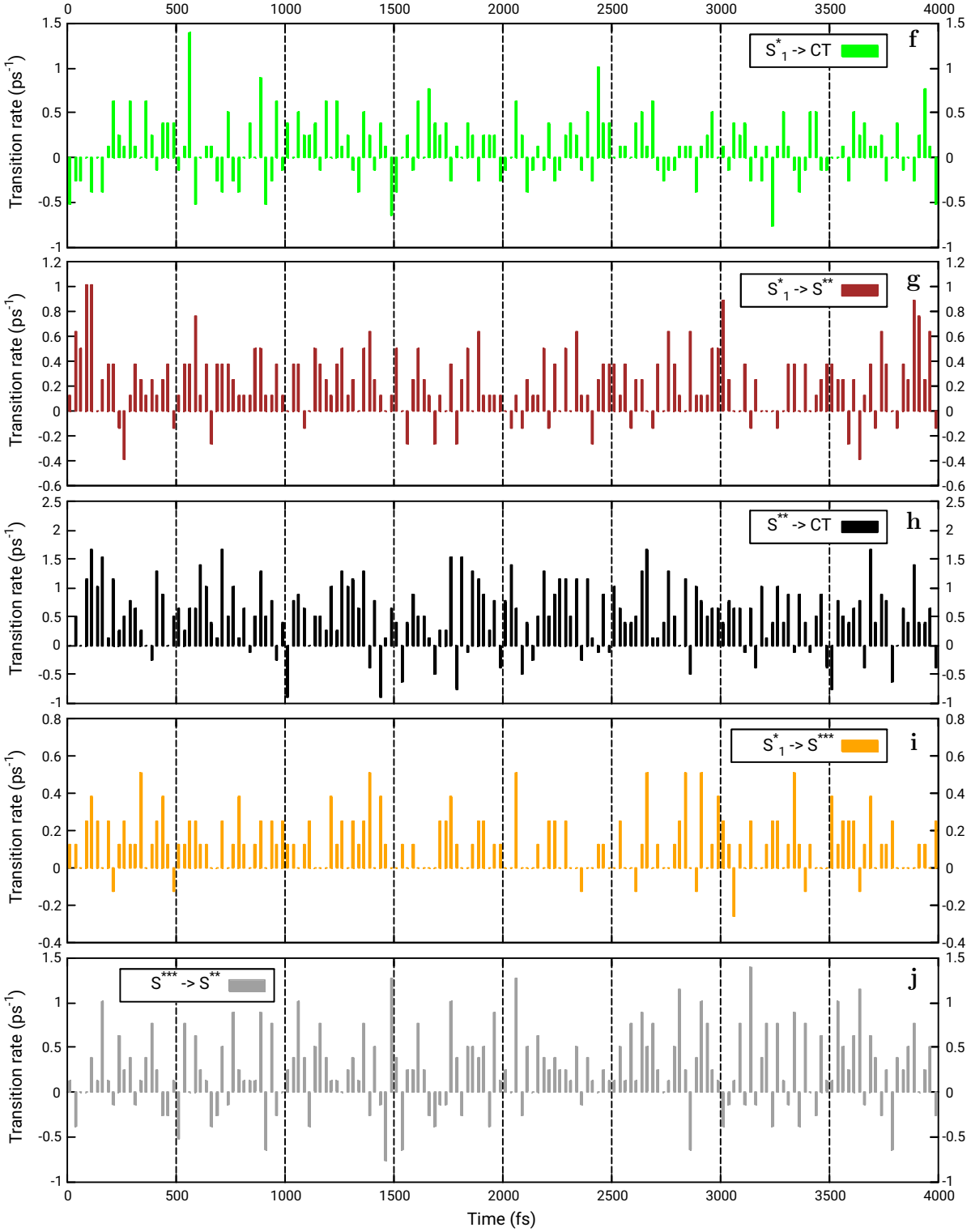

Figure S8: Net transition rates (in $ps^{-1}$) between pairs of states as functions of time (fs), obtained from the simulation of the excited state dynamics for dimer **D2** of ML-DPBF. The $CT_n$ states, the higher excitonic states $S_1^{**}$ and $S_2^{**}$, and $S_1^{***}$ and $S_2^{***}$ are grouped together and indicated as $CT$, $S^{**}$ and $S^{***}$, respectively. Each rate is defined as $\frac{\#\ transitions}{\#\ trajectories\ \cdot\ time\ interval}$. For each type of transition, one bar represents a net transition rate computed in a time interval of 25 fs (e.g. the first bar corresponds to the interval $(0{:}25]$ fs). For panels f-j, see the next page.

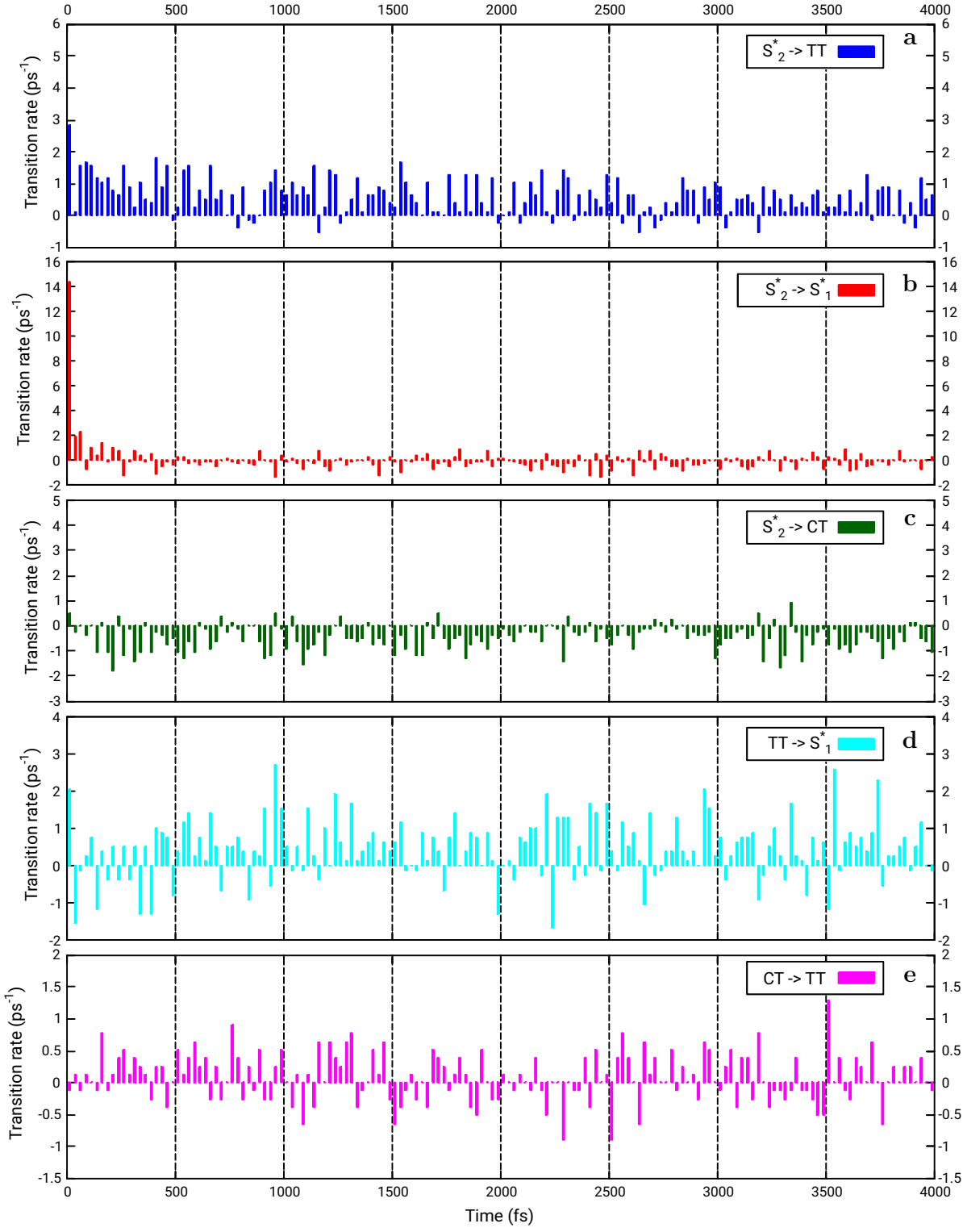

Figure S8: (continued from previous page)

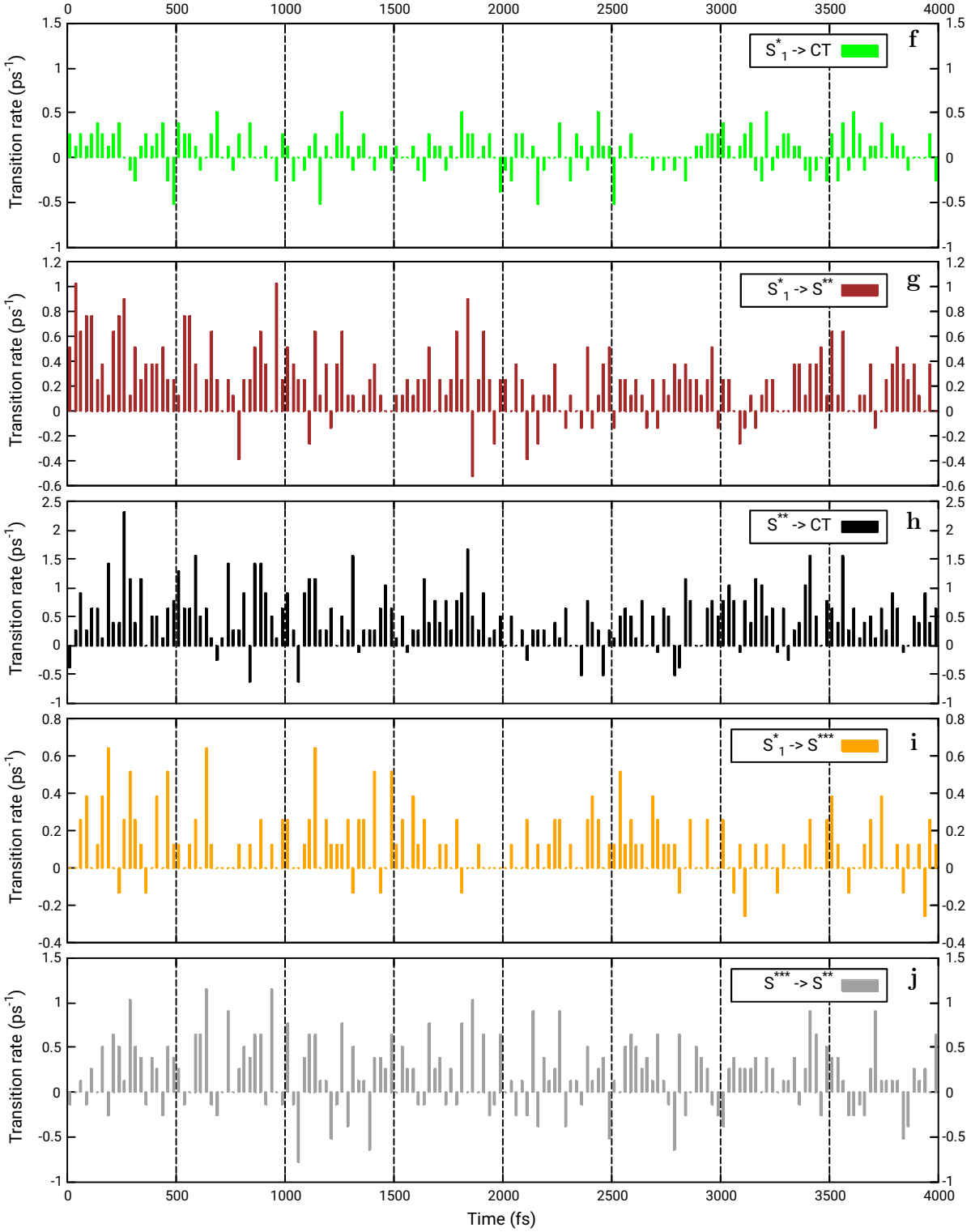

Table S10: Comparison of the stacking ($D$) and slip ($d$) distances between chromophores at the starting time ($t$ = 0, $X_0$), at the transitions between pairs of states ($X_t$), and in the double triplet state $TT$ ($X_{TT}$), averaged over all trajectories, obtained in the first 4 ps of the simulations of the excited state dynamics for dimers **D1** and **D2** of ML-DPBF. All distances are reported in units of Å.

| Geom. | Dimer **D1** | | Dimer **D2** | |
|---|---|---|---|---|
| | $D$ [a] | $d$ [b] | $D$ [a] | $d$ [b] |
| $X_0$ | 3.7705 | 1.1104 | 3.6513 | 4.2530 |
| $\boldsymbol{S_2^* \rightarrow TT}$ | | | | |
| $X_t$ | 3.7217 | 1.1908 | 3.5803 | 3.9227 |
| $X_t - X_0$ | -0.0488 | 0.0804 | -0.0710 | -0.3303 |
| $\boldsymbol{CT_1 \rightarrow TT}$ | | | | |
| $X_t$ | 3.6639 | 1.2032 | 3.5568 | 3.7372 |
| $X_t - X_0$ | -0.1066 | 0.0928 | -0.0945 | -0.5158 |
| $\boldsymbol{CT_2 \rightarrow TT}$ | | | | |
| $X_t$ | 3.6389 | 1.1609 | 3.5379 | 3.7519 |
| $X_t - X_0$ | -0.1316 | 0.0505 | -0.1134 | -0.5011 |
| $\boldsymbol{TT \rightarrow S_1^*}$ | | | | |
| $X_t$ | 3.6941 | 1.1723 | 3.5781 | 3.8436 |
| $X_t - X_0$ | -0.0764 | 0.0619 | -0.0732 | -0.4094 |
| $\boldsymbol{TT}$ | | | | |
| $X_{TT}$ | 3.7361 | 1.1624 | 3.6135 | 3.8899 |
| $X_{TT} - X_0$ | -0.0344 | 0.0520 | -0.0378 | -0.3631 |

[a] $D$ is the average distance (in Å) beween the centroid of one chromophore and its projection to the best-fit plane of the other chromophore.

[b] $d$ is the average distance (in Å) beween the centroid of one chromophore and the centroid projection of the other chromophore to the best-fit plane of the first chromophore.

Table S11: Average values (diagonal and lower triangular part) and standard deviations (upper triangular part) of the electronic Hamiltonian matrix elements in the excitonic basis at the geometries where the current adiabatic wavefunction is dominated by the $TT$ state, obtained from the simulations of the excited state dynamics for dimers **D1** and **D2** of ML-DPBF.

Dimer **D1**

| $\hat{\mathcal{H}}_{el}$ | $S_0S_0$ | $S_1^*$ | $S_2^*$ | $TT$ | $CT_1$ | $CT_2$ | $S_1^{**}$ | $S_2^{**}$ | $S_1^{***}$ | $S_2^{***}$ |
|---|---|---|---|---|---|---|---|---|---|---|
| $S_0S_0$ | 0.00 | ± 63.12 | ± 93.34 | ± 3.20 | ± 75.73 | ± 67.58 | ± 123.11 | ± 89.38 | ± 125.61 | ± 111.42 |
| $S_1^*$ | 0.16 | 2255.02 | ± 0.00 | ± 2.82 | ± 64.83 | ± 70.44 | ± 88.37 | ± 79.06 | ± 155.76 | ± 114.60 |
| $S_2^*$ | 0.20 | 0.00 | 2657.23 | ± 7.45 | ± 52.76 | ± 51.95 | ± 141.07 | ± 125.82 | ± 102.47 | ± 140.01 |
| $TT$ | 0.00 | 0.00 | 0.01 | 1948.35 | ± 76.00 | ± 70.27 | ± 5.88 | ± 4.74 | ± 4.28 | ± 4.51 |
| $CT_1$ | 0.01 | -0.10 | -0.03 | -0.01 | 2533.57 | ± 0.00 | ± 15.99 | ± 14.66 | ± 15.47 | ± 13.42 |
| $CT_2$ | 0.05 | 0.03 | 0.01 | 0.00 | 0.00 | 2663.76 | ± 14.49 | ± 13.64 | ± 12.75 | ± 14.07 |
| $S_1^{**}$ | -5.86 | 0.04 | -0.05 | 0.00 | -0.01 | 0.01 | 2791.36 | ± 0.00 | ± 65.96 | ± 48.06 |
| $S_2^{**}$ | -0.74 | 0.04 | 0.32 | -0.01 | 0.00 | 0.01 | 0.00 | 2947.85 | ± 52.19 | ± 50.37 |
| $S_1^{***}$ | -5.47 | 0.28 | -0.09 | 0.00 | 0.03 | -0.03 | 2.67 | 1.18 | 2960.70 | ± 0.00 |
| $S_2^{***}$ | -0.96 | 0.19 | -0.26 | 0.00 | 0.01 | 0.01 | 1.19 | 1.03 | 0.00 | 3146.48 |

Dimer **D2**

| $\hat{\mathcal{H}}_{el}$ | $S_0S_0$ | $S_1^*$ | $S_2^*$ | $TT$ | $CT_1$ | $CT_2$ | $S_1^{**}$ | $S_2^{**}$ | $S_1^{***}$ | $S_2^{***}$ |
|---|---|---|---|---|---|---|---|---|---|---|
| $S_0S_0$ | 0.00 | ± 100.84 | ± 72.26 | ± 3.36 | ± 71.20 | ± 72.63 | ± 122.22 | ± 62.89 | ± 114.99 | ± 62.59 |
| $S_1^*$ | 0.02 | 2359.81 | ± 0.00 | ± 5.28 | ± 68.77 | ± 68.06 | ± 155.45 | ± 126.96 | ± 127.44 | ± 145.10 |
| $S_2^*$ | -0.02 | 0.00 | 2579.93 | ± 3.04 | ± 58.20 | ± 60.83 | ± 74.33 | ± 90.12 | ± 116.75 | ± 129.74 |
| $TT$ | 0.00 | -0.01 | 0.00 | 1955.51 | ± 72.36 | ± 65.75 | ± 7.04 | ± 5.94 | ± 5.42 | ± 6.61 |
| $CT_1$ | 0.05 | -0.08 | 0.01 | 0.04 | 2660.93 | ± 0.00 | ± 27.47 | ± 28.06 | ± 33.42 | ± 29.88 |
| $CT_2$ | -0.01 | 0.13 | 0.13 | 0.07 | 0.00 | 2785.15 | ± 25.32 | ± 27.32 | ± 28.51 | ± 36.17 |
| $S_1^{**}$ | -3.36 | -0.02 | 0.00 | -0.01 | 0.00 | 0.01 | 2803.68 | ± 0.00 | ± 71.97 | ± 45.67 |
| $S_2^{**}$ | -0.06 | -0.11 | -0.05 | -0.01 | -0.01 | 0.01 | 0.00 | 2966.61 | ± 43.28 | ± 49.91 |
| $S_1^{***}$ | -5.68 | -0.16 | -0.01 | 0.00 | -0.06 | 0.00 | 2.78 | 0.84 | 2958.02 | ± 0.00 |
| $S_2^{***}$ | -0.01 | 0.02 | 0.00 | 0.00 | -0.03 | 0.05 | 0.80 | 0.85 | 0.00 | 3139.76 |

Table S12: Results obtained from the fitting of the $TT$ and $S_0S_0$ populations for dimers **D1** and **D2** of ML-DPBF, in the time interval of 4-8 ps (see Figure 6, in the main text). The fitting functions are $P_{TT}(t) = P_{TT}(t_0) + a\ (1 - e^{-(t-t_0)/\tau})$ and $P_{S_0S_0}(t) = P_{S_0S_0}(t_0) + b\ (1 - e^{-(t-t_0)/\tau})$, with $t_0 = 4$ ps. $\tau$ was determined by fitting the $TT$ population only. The asymptotic populations $P_{TT}(\infty)$, $P_{S_0S_0}(\infty)$ and $P_X(\infty)$ are also reported ($X$ stands for all the excited states included in the dynamics treatment, except $TT$).

| Dimer | $P_{TT}(t_0)$ | $P_{S_0S_0}(t_0)$ | $\tau$ (ps) | $a$ | $b$ | $P_{TT}(\infty)$ | $P_{S_0S_0}(\infty)$ | $P_X(\infty)$ |
|---|---|---|---|---|---|---|---|---|
| **D1** | 0.550 | 0.019 | 0.769 | 0.188 | 0.010 | 0.738 | 0.030 | 0.232 |
| **D2** | 0.691 | 0.029 | 0.704 | 0.152 | 0.008 | 0.843 | 0.037 | 0.120 |

# S3 Linear dimer D0

## S3.1 Ground state thermal equilibration

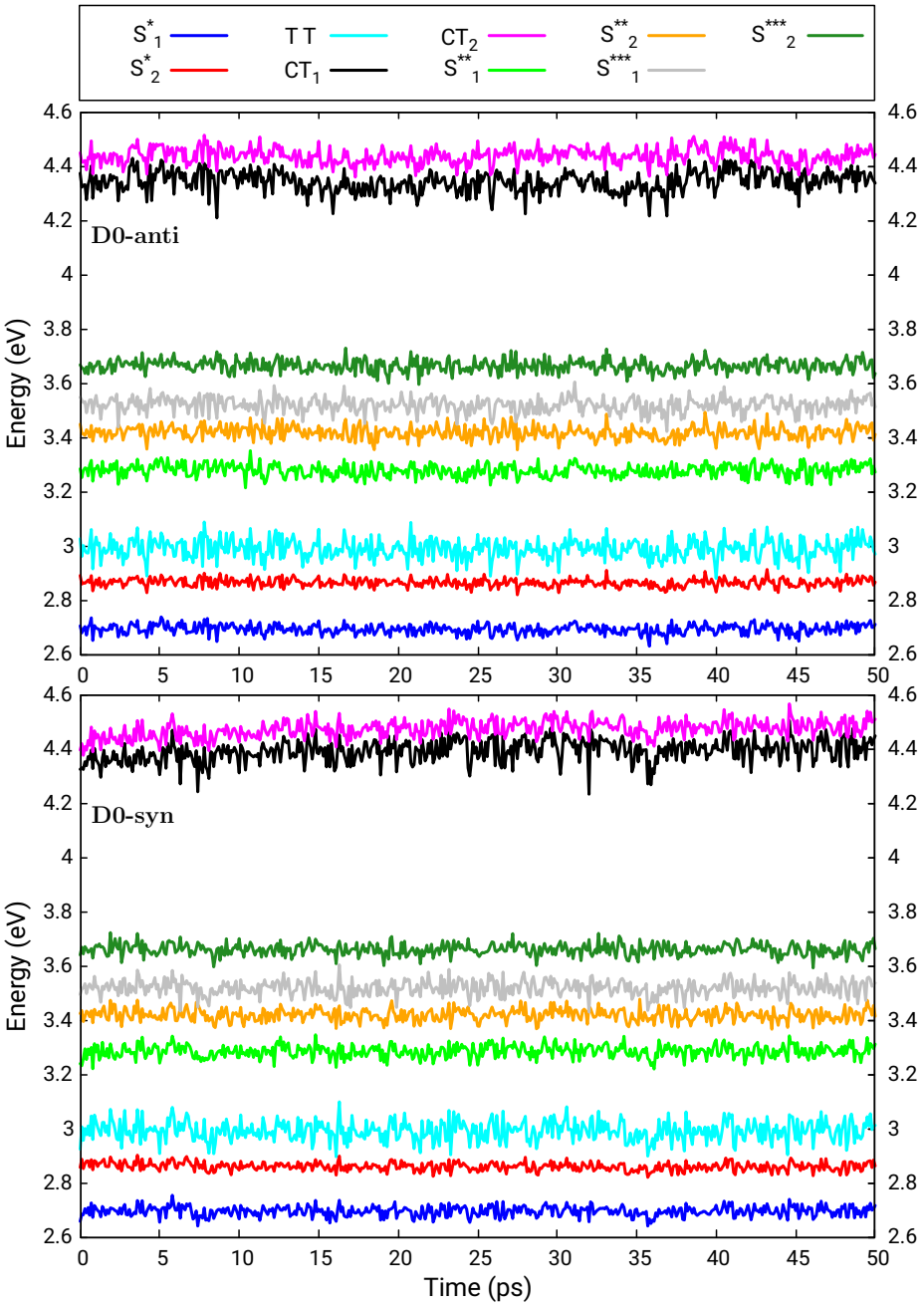


Figure S9: Excitation energies (in eV) from the ground state ($S_0S_0$) in the excitonic representation, obtained from the ground state thermal equilibrations for two conformers of dimer **D0** of ML-DPBF, namely **D0-anti** (upper panel) and **D0-syn** (lower panel). Each point in the plot is obtained by averaging over a time interval of 100 fs.

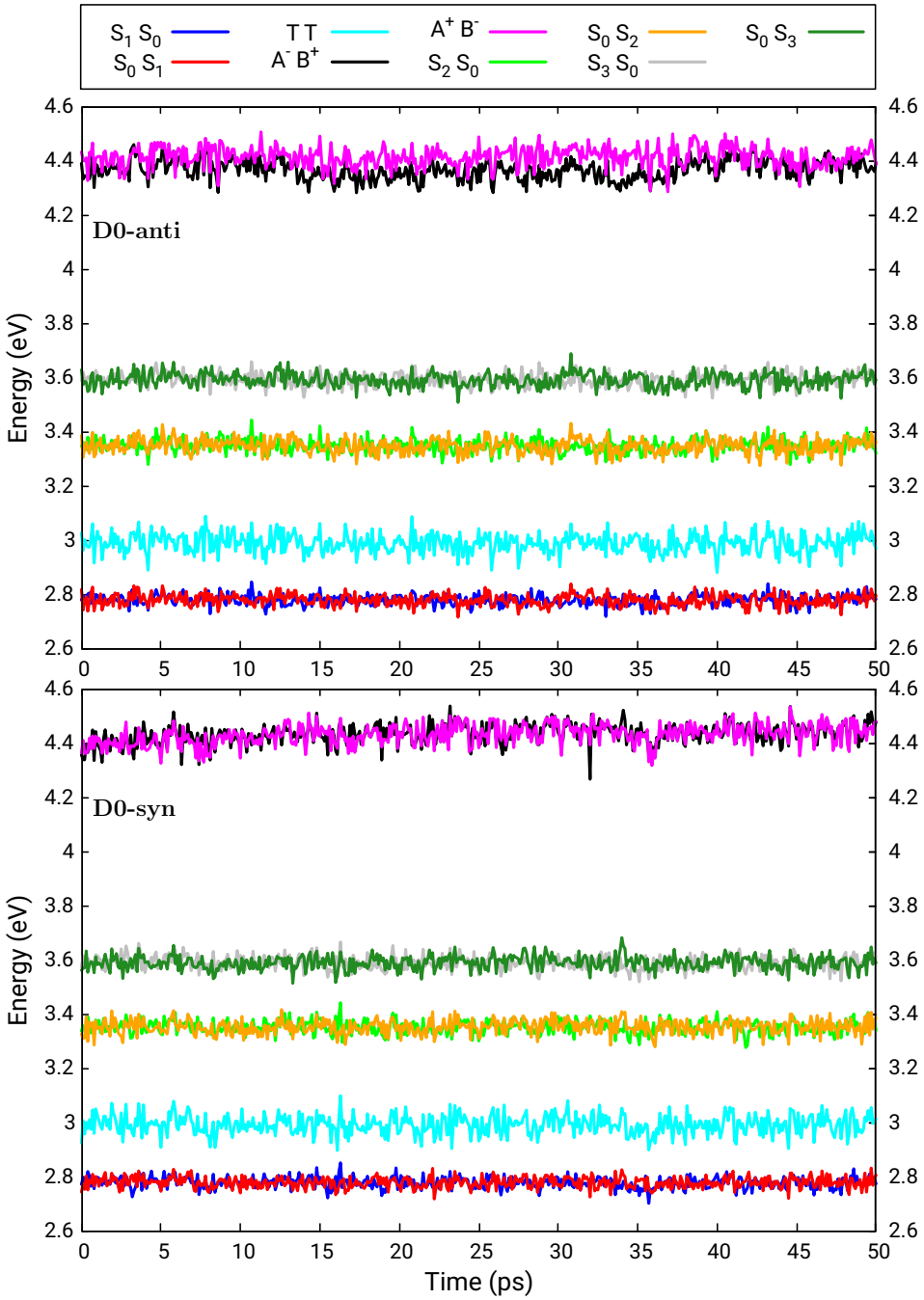


Figure S10: Excitation energies (in eV) from the ground state ($S_0S_0$) in the diabatic representation, obtained from the ground state thermal equilibrations for two conformers of dimer **D0** of ML-DPBF, namely **D0-anti** (upper panel) and **D0-syn** (lower panel). Each point in the plot is obtained by averaging over a time interval of 100 fs.

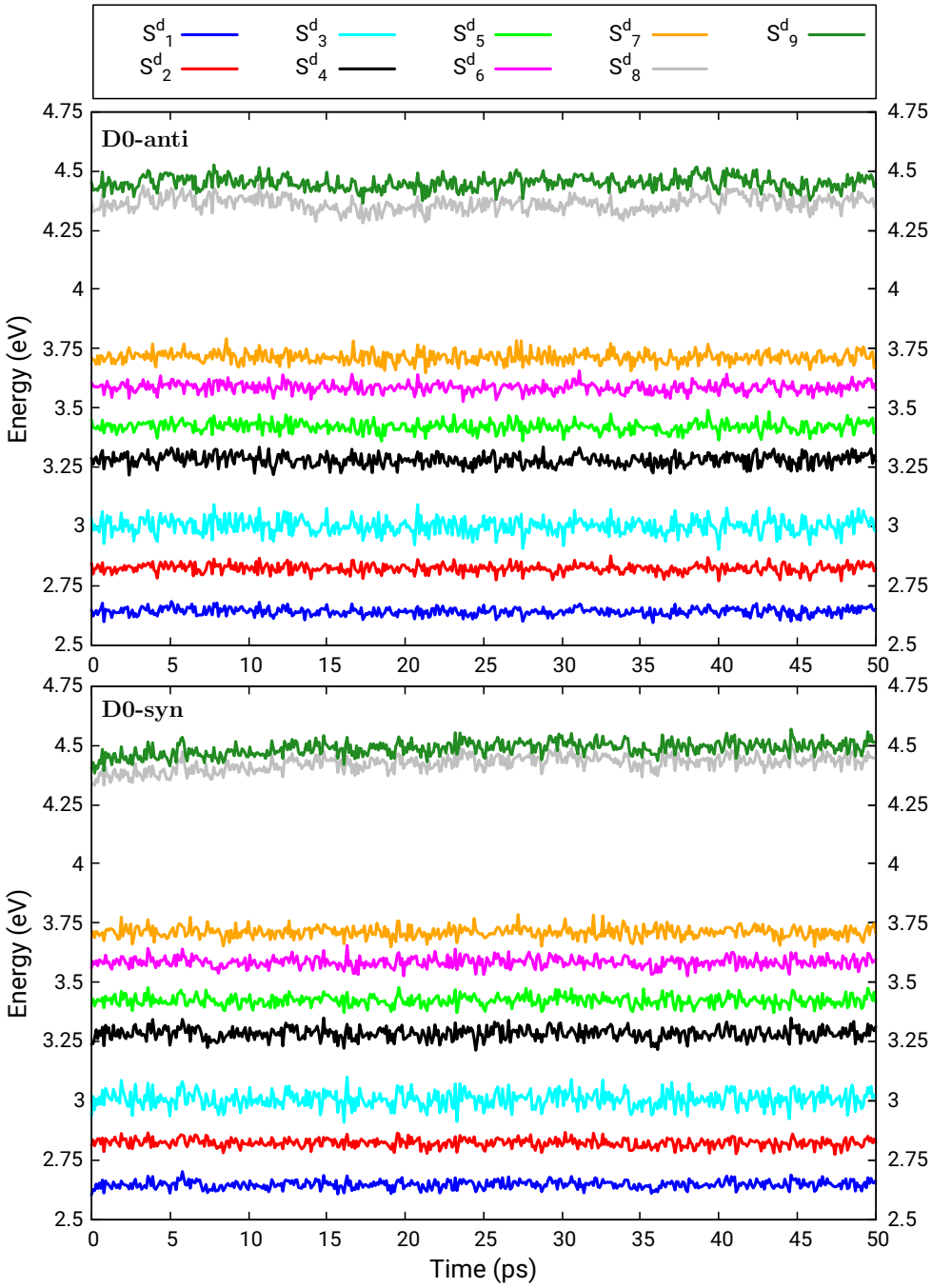


Figure S11: Excitation energies (in eV) from the ground state ($S_0^d$) in the adiabatic representation, obtained from the ground state thermal equilibrations for two conformers of dimer **D0** of ML-DPBF, namely **D0-anti** (upper panel) and **D0-syn** (lower panel). A superscript $d$ is added to the state labels to indicate that they are the adiabatic states of the dimer. Each point in the plot is obtained by averaging over a time interval of 100 fs.

Table S13: Average values (diagonal and lower triangular part) and standard deviations (upper triangular part) of the electronic Hamiltonian matrix elements for the excitonic basis obtained from the ground state thermal equilibration of two conformers of dimer **D0** of ML-DPBF, namely **D0-anti** (upper panel) and **D0-syn** (lower panel). All matrix elements are in units of meV. Averaging time interval: 30-50 ps.

Dimer **D0-anti**

| $\hat{\mathcal{H}}_{el}$ | $S_0S_0$ | $S_1^*$ | $S_2^*$ | $TT$ | $CT_1$ | $CT_2$ | $S_1^{**}$ | $S_2^{**}$ | $S_1^{***}$ | $S_2^{***}$ |
|---|---|---|---|---|---|---|---|---|---|---|
| $S_0S_0$ | 0.00 | ± 32.55 | ± 31.35 | ± 1.05 | ± 129.03 | ± 33.54 | ± 49.70 | ± 52.51 | ± 28.86 | ± 20.49 |
| $S_1^*$ | 0.40 | 2692.72 | ± 0.00 | ± 0.17 | ± 22.40 | ± 17.50 | ± 64.75 | ± 41.68 | ± 185.66 | ± 105.72 |
| $S_2^*$ | 19.85 | 0.00 | 2862.40 | ± 0.11 | ± 8.10 | ± 7.94 | ± 32.07 | ± 38.44 | ± 84.65 | ± 151.86 |
| $TT$ | 0.16 | -0.05 | 0.02 | 2988.03 | ± 11.94 | ± 17.99 | ± 0.83 | ± 0.62 | ± 0.45 | ± 0.40 |
| $CT_1$ | -0.98 | 1.10 | -0.64 | -0.07 | 4346.81 | ± 0.00 | ± 83.08 | ± 39.01 | ± 41.54 | ± 9.34 |
| $CT_2$ | -2.22 | 1.40 | -0.68 | 1.19 | 0.00 | 4440.71 | ± 23.45 | ± 10.33 | ± 12.64 | ± 11.88 |
| $S_1^{**}$ | -1.22 | 4.75 | -0.39 | 0.01 | -7.63 | 0.26 | 3278.44 | ± 0.00 | ± 26.60 | ± 14.81 |
| $S_2^{**}$ | -0.13 | -1.25 | 0.77 | 0.03 | -0.85 | -0.03 | 0.00 | 3414.83 | ± 17.84 | ± 22.24 |
| $S_1^{***}$ | 0.54 | 7.87 | 3.47 | 0.01 | 0.80 | 0.31 | 0.41 | -0.44 | 3519.07 | ± 0.00 |
| $S_2^{***}$ | 0.14 | 2.37 | 17.76 | 0.03 | 0.46 | 0.37 | 0.39 | -0.67 | 0.00 | 3662.81 |

Dimer **D0-syn**

| $\hat{\mathcal{H}}_{el}$ | $S_0S_0$ | $S_1^*$ | $S_2^*$ | $TT$ | $CT_1$ | $CT_2$ | $S_1^{**}$ | $S_2^{**}$ | $S_1^{***}$ | $S_2^{***}$ |
|---|---|---|---|---|---|---|---|---|---|---|
| $S_0S_0$ | 0.00 | ± 32.81 | ± 30.82 | ± 2.17 | ± 171.51 | ± 30.28 | ± 51.37 | ± 49.15 | ± 28.37 | ± 20.53 |
| $S_1^*$ | -1.12 | 2694.39 | ± 0.00 | ± 0.34 | ± 33.02 | ± 23.81 | ± 61.91 | ± 39.89 | ± 182.85 | ± 101.83 |
| $S_2^*$ | 13.75 | 0.00 | 2856.77 | ± 0.15 | ± 11.66 | ± 8.81 | ± 32.05 | ± 39.05 | ± 80.59 | ± 150.69 |
| $TT$ | -0.36 | 0.10 | 0.10 | 2990.85 | ± 19.31 | ± 25.38 | ± 1.56 | ± 0.82 | ± 0.67 | ± 0.25 |
| $CT_1$ | 2.76 | -0.19 | -0.24 | -0.10 | 4400.90 | ± 0.00 | ± 111.99 | ± 62.47 | ± 50.26 | ± 10.19 |
| $CT_2$ | -0.27 | -0.04 | -0.18 | -0.94 | 0.00 | 4482.11 | ± 24.57 | ± 10.56 | ± 11.13 | ± 9.79 |
| $S_1^{**}$ | 1.41 | -3.87 | 0.71 | 0.01 | -7.78 | -0.69 | 3285.42 | ± 0.00 | ± 26.76 | ± 14.30 |
| $S_2^{**}$ | 1.11 | -0.58 | -0.53 | 0.02 | -2.82 | 0.07 | 0.00 | 3418.20 | ± 17.48 | ± 23.18 |
| $S_1^{***}$ | 0.58 | 12.25 | 5.04 | -0.01 | -1.18 | 0.37 | -0.89 | -0.23 | 3516.39 | ± 0.00 |
| $S_2^{***}$ | 0.29 | 3.85 | 13.69 | 0.00 | -0.14 | -0.05 | -0.09 | -0.02 | 0.00 | 3659.50 |

Table S14: Average values (diagonal and lower triangular part) and standard deviations (upper triangular part) of the electronic Hamiltonian matrix elements for the diabatic basis obtained from the ground state thermal equilibration of two conformers of dimer **D0** of ML-DPBF, namely **D0-anti** (upper panel) and **D0-syn** (lower panel). All matrix elements are in units of meV. Time interval: 30-50 ps.

Dimer **D0-anti**

| $\hat{\mathcal{H}}_{el}$ | $S_0S_0$ | $S_1S_0$ | $S_0S_1$ | $TT$ | $A^-B^+$ | $A^+B^-$ | $S_2S_0$ | $S_0S_2$ | $S_3S_0$ | $S_0S_3$ |
|---|---|---|---|---|---|---|---|---|---|---|
| $S_0S_0$ | 0.00 | ± 31.32 | ± 31.55 | ± 1.05 | ± 61.42 | ± 118.28 | ± 50.20 | ± 51.94 | ± 25.22 | ± 24.83 |
| $S_1S_0$ | 15.19 | 2777.62 | ± 6.13 | ± 0.14 | ± 12.74 | ± 16.04 | ± 56.64 | ± 34.62 | ± 190.54 | ± 21.26 |
| $S_0S_1$ | 15.15 | 66.92 | 2777.50 | ± 0.15 | ± 17.47 | ± 13.81 | ± 33.40 | ± 54.16 | ± 20.47 | ± 194.18 |
| $TT$ | 0.16 | 0.05 | -0.03 | 2988.03 | ± 13.74 | ± 16.46 | ± 0.73 | ± 0.73 | ± 0.41 | ± 0.44 |
| $A^-B^+$ | 1.63 | -1.73 | 3.33 | -1.85 | 4370.71 | ± 8.69 | ± 37.68 | ± 23.37 | ± 18.87 | ± 17.93 |
| $A^+B^-$ | 3.80 | -2.62 | 2.12 | 2.19 | -1.46 | 4416.81 | ± 49.63 | ± 68.05 | ± 24.49 | ± 28.62 |
| $S_2S_0$ | 2.30 | -0.72 | 1.32 | 0.01 | -2.23 | -3.62 | 3346.47 | ± 17.47 | ± 26.82 | ± 11.46 |
| $S_0S_2$ | -2.48 | -1.68 | 1.15 | -0.11 | -1.08 | -7.87 | 2.32 | 3346.80 | ± 12.00 | ± 27.00 |
| $S_3S_0$ | -0.40 | -35.57 | 3.26 | -0.07 | -0.38 | 2.78 | -0.98 | 1.60 | 3590.04 | ± 7.58 |
| $S_0S_3$ | -0.45 | 0.65 | -10.55 | -0.04 | -3.21 | 0.19 | -3.61 | 1.20 | 2.21 | 3591.83 |

Dimer **D0-syn**

| $\hat{\mathcal{H}}_{el}$ | $S_0S_0$ | $S_1S_0$ | $S_0S_1$ | $TT$ | $A^-B^+$ | $A^+B^-$ | $S_2S_0$ | $S_0S_2$ | $S_3S_0$ | $S_0S_3$ |
|---|---|---|---|---|---|---|---|---|---|---|
| $S_0S_0$ | 0.00 | ± 31.76 | ± 31.22 | ± 2.17 | ± 120.12 | ± 126.12 | ± 50.65 | ± 49.10 | ± 25.03 | ± 24.49 |
| $S_1S_0$ | 11.50 | 2774.28 | ± 5.79 | ± 0.25 | ± 21.58 | ± 20.61 | ± 55.09 | ± 31.38 | ± 190.68 | ± 19.78 |
| $S_0S_1$ | 10.07 | 61.87 | 2776.88 | ± 0.28 | ± 18.02 | ± 25.50 | ± 31.30 | ± 54.05 | ± 20.53 | ± 179.59 |
| $TT$ | -0.36 | -0.01 | 0.14 | 2990.85 | ± 20.95 | ± 23.99 | ± 1.26 | ± 1.22 | ± 0.52 | ± 0.50 |
| $A^-B^+$ | -2.27 | 1.43 | -1.06 | 1.43 | 4441.58 | ± 16.41 | ± 68.89 | ± 58.93 | ± 25.22 | ± 25.21 |
| $A^+B^-$ | 1.10 | -0.93 | 1.03 | 1.09 | -3.02 | 4441.43 | ± 69.04 | ± 64.23 | ± 29.86 | ± 26.21 |
| $S_2S_0$ | -8.32 | 3.28 | -6.89 | -0.15 | -7.06 | -5.25 | 3349.86 | ± 16.12 | ± 27.42 | ± 11.18 |
| $S_0S_2$ | 3.55 | 3.06 | -2.20 | 0.16 | -1.75 | -6.20 | -1.13 | 3353.76 | ± 10.81 | ± 27.62 |
| $S_3S_0$ | 0.51 | 7.42 | -0.51 | 0.03 | -0.27 | -0.40 | 0.94 | 1.79 | 3585.99 | ± 7.57 |
| $S_0S_3$ | 0.31 | 6.64 | -62.13 | 0.01 | -0.27 | -0.41 | -0.96 | -1.70 | -0.73 | 3589.91 |

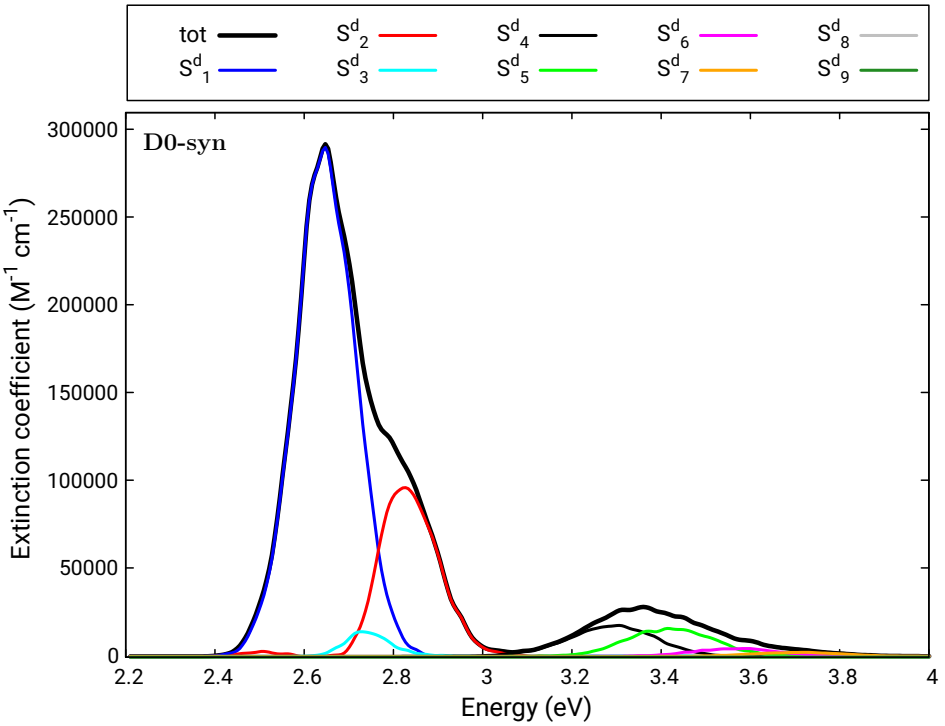


Figure S12: Absorption spectrum obtained from the ground state thermal equilibration for dimer **D0-syn** of ML-DPBF. Averaging time interval: 30-50 ps.

Table S15: Average weights (square coefficients) of the excitonic states in the 10 low-lying adiabatic states obtained in the thermal equilibrations on $S_0^d$ for two conformers of dimer **D0** of ML-DPBF, namely **D0-anti** (upper panel) and **D0-syn** (lower panel). Weights > 0.1 are in bold. The relative energies (in eV) of the adiabatic states and the transition dipole moments squared (a.u.) for the adiabatic and the excitonic states are also reported. Averaging time interval: 30-50 ps.

Dimer **D0-anti**

| | $S_0S_0$ | $S_1^*$ | $S_2^*$ | $TT$ | $CT_1$ | $CT_2$ | $S_1^{**}$ | $S_2^{**}$ | $S_1^{***}$ | $S_2^{***}$ | Energy (eV) | $\mu^2_{S_0^d \to S_n^d}$ (a.u.) |
|---|---|---|---|---|---|---|---|---|---|---|---|---|
| $S_0^d$ | **0.998** | 0.000 | 0.000 | 0.000 | 0.001 | 0.000 | 0.000 | 0.000 | 0.000 | 0.000 | 0.000 | - |
| $S_1^d$ | 0.000 | **0.931** | 0.001 | 0.003 | 0.000 | 0.000 | 0.009 | 0.003 | 0.042 | 0.010 | 2.640 | 26.321 |
| $S_2^d$ | 0.000 | 0.004 | **0.848** | **0.101** | 0.000 | 0.000 | 0.004 | 0.003 | 0.011 | 0.029 | 2.821 | 6.300 |
| $S_3^d$ | 0.000 | 0.000 | 0.097 | **0.884** | 0.000 | 0.000 | 0.012 | 0.001 | 0.001 | 0.004 | 3.001 | 0.791 |
| $S_4^d$ | 0.000 | 0.006 | 0.005 | 0.012 | 0.008 | 0.000 | **0.936** | 0.009 | 0.023 | 0.002 | 3.280 | 2.634 |
| $S_5^d$ | 0.000 | 0.008 | 0.004 | 0.000 | 0.000 | 0.000 | 0.015 | **0.888** | 0.076 | 0.009 | 3.418 | 1.674 |
| $S_6^d$ | 0.000 | 0.037 | 0.016 | 0.000 | 0.000 | 0.000 | 0.016 | 0.085 | **0.828** | 0.019 | 3.585 | 0.398 |
| $S_7^d$ | 0.000 | 0.014 | 0.031 | 0.000 | 0.000 | 0.000 | 0.002 | 0.010 | 0.017 | **0.928** | 3.712 | 0.226 |
| $S_8^d$ | 0.000 | 0.000 | 0.000 | 0.000 | **0.961** | 0.037 | 0.001 | 0.000 | 0.001 | 0.000 | 4.366 | 0.006 |
| $S_9^d$ | 0.001 | 0.000 | 0.000 | 0.000 | 0.029 | **0.962** | 0.005 | 0.001 | 0.001 | 0.000 | 4.453 | 0.024 |
| $\mu^2_{0\to i(dia.)}$ (a.u.) | - | 24.651 | 6.634 | 0.006 | 0.065 | 0.035 | 2.839 | 1.843 | 1.535 | 0.752 | - | - |

Dimer **D0-syn**

| | $S_0S_0$ | $S_1^*$ | $S_2^*$ | $TT$ | $CT_1$ | $CT_2$ | $S_1^{**}$ | $S_2^{**}$ | $S_1^{***}$ | $S_2^{***}$ | Energy (eV) | $\mu^2_{S_0^d \to S_n^d}$ (a.u.) |
|---|---|---|---|---|---|---|---|---|---|---|---|---|
| $S_0$ | **0.998** | 0.000 | 0.000 | 0.000 | 0.002 | 0.000 | 0.000 | 0.000 | 0.000 | 0.000 | 0.000 | - |
| $S_1$ | 0.000 | **0.931** | 0.001 | 0.005 | 0.000 | 0.000 | 0.009 | 0.003 | 0.042 | 0.010 | 2.646 | 25.818 |
| $S_2$ | 0.000 | 0.006 | **0.855** | 0.093 | 0.000 | 0.000 | 0.004 | 0.003 | 0.010 | 0.028 | 2.819 | 7.935 |
| $S_3$ | 0.000 | 0.000 | 0.092 | **0.885** | 0.001 | 0.000 | 0.016 | 0.001 | 0.001 | 0.004 | 3.006 | 0.933 |
| $S_4$ | 0.000 | 0.006 | 0.004 | 0.016 | 0.015 | 0.000 | **0.919** | 0.016 | 0.022 | 0.002 | 3.282 | 1.833 |
| $S_5$ | 0.000 | 0.008 | 0.004 | 0.000 | 0.000 | 0.000 | 0.020 | **0.870** | 0.087 | 0.009 | 3.422 | 1.581 |
| $S_6$ | 0.000 | 0.035 | 0.014 | 0.000 | 0.000 | 0.000 | 0.019 | 0.093 | **0.816** | 0.022 | 3.583 | 0.413 |
| $S_7$ | 0.000 | 0.013 | 0.030 | 0.000 | 0.000 | 0.000 | 0.002 | 0.011 | 0.019 | **0.925** | 3.711 | 0.217 |
| $S_8$ | 0.001 | 0.000 | 0.000 | 0.000 | **0.935** | 0.057 | 0.004 | 0.001 | 0.001 | 0.000 | 4.436 | 0.020 |
| $S_9$ | 0.001 | 0.000 | 0.000 | 0.000 | 0.046 | **0.942** | 0.006 | 0.003 | 0.002 | 0.000 | 4.497 | 0.033 |
| $\mu^2_{0\to i(dia.)}$ (a.u.) | - | 24.307 | 8.254 | 0.006 | 0.112 | 0.047 | 2.058 | 1.771 | 1.495 | 0.767 | - | - |

Table S16: Average weights (square coefficients) of the diabatic states in the 10 low-lying adiabatic states obtained in the thermal equilibrations on $S_0^d$ for two conformers of dimer **D0** of ML-DPBF, namely **D0-anti** (upper panel) and **D0-syn** (lower panel). Weights > 0.1 are in bold. The relative energies (in eV) of the adiabatic states and the transition dipole moments squared (a.u.) for the adiabatic and the excitonic states are also reported. Averaging time interval: 30-50 ps.

Dimer **D0-anti**

| | $S_0S_0$ | $S_1S_0$ | $S_0S_1$ | $TT$ | $A^-B^+$ | $A^+B^-$ | $S_2S_0$ | $S_0S_2$ | $S_3S_0$ | $S_0S_3$ | Energy (eV) | $\mu^2_{S_0^d \to S_n^d}$ (a.u.) |
|---|---|---|---|---|---|---|---|---|---|---|---|---|
| $S_0^d$ | **0.998** | 0.000 | 0.000 | 0.000 | 0.000 | 0.001 | 0.000 | 0.000 | 0.000 | 0.000 | 0.000 | - |
| $S_1^d$ | 0.000 | **0.466** | **0.466** | 0.003 | 0.000 | 0.000 | 0.006 | 0.006 | 0.026 | 0.026 | 2.640 | 26.321 |
| $S_2^d$ | 0.000 | **0.425** | **0.426** | **0.101** | 0.000 | 0.000 | 0.004 | 0.004 | 0.020 | 0.020 | 2.821 | 6.300 |
| $S_3^d$ | 0.000 | 0.049 | 0.048 | **0.884** | 0.000 | 0.000 | 0.008 | 0.005 | 0.003 | 0.003 | 3.001 | 0.791 |
| $S_4^d$ | 0.000 | 0.005 | 0.005 | 0.012 | 0.002 | 0.007 | **0.471** | **0.473** | 0.014 | 0.011 | 3.280 | 2.634 |
| $S_5^d$ | 0.000 | 0.006 | 0.006 | 0.000 | 0.000 | 0.000 | **0.449** | **0.454** | 0.042 | 0.042 | 3.418 | 1.674 |
| $S_6^d$ | 0.000 | 0.027 | 0.026 | 0.000 | 0.000 | 0.000 | 0.053 | 0.048 | **0.429** | **0.418** | 3.585 | 0.398 |
| $S_7^d$ | 0.000 | 0.022 | 0.022 | 0.000 | 0.000 | 0.000 | 0.006 | 0.005 | **0.466** | **0.479** | 3.712 | 0.226 |
| $S_8^d$ | 0.000 | 0.000 | 0.000 | 0.000 | **0.715** | **0.282** | 0.001 | 0.001 | 0.000 | 0.000 | 4.366 | 0.006 |
| $S_9^d$ | 0.001 | 0.000 | 0.000 | 0.000 | **0.282** | **0.709** | 0.002 | 0.004 | 0.001 | 0.001 | 4.453 | 0.024 |
| $\mu^2_{0\to i(dia.)}$ (a.u.) | - | 15.588 | 15.696 | 0.006 | 0.035 | 0.065 | 2.178 | 2.504 | 1.135 | 1.152 | - | - |

Dimer **D0-syn**

| | $S_0S_0$ | $S_1S_0$ | $S_0S_1$ | $TT$ | $A^-B^+$ | $A^+B^-$ | $S_2S_0$ | $S_0S_2$ | $S_3S_0$ | $S_0S_3$ | Energy (eV) | $\mu^2_{S_0^d \to S_n^d}$ (a.u.) |
|---|---|---|---|---|---|---|---|---|---|---|---|---|
| $S_0$ | **0.998** | 0.000 | 0.000 | 0.000 | 0.001 | 0.001 | 0.000 | 0.000 | 0.000 | 0.000 | 0.000 | - |
| $S_1$ | 0.000 | **0.473** | **0.458** | 0.005 | 0.000 | 0.000 | 0.006 | 0.006 | 0.026 | 0.025 | 2.646 | 25.818 |
| $S_2$ | 0.000 | **0.424** | **0.437** | 0.093 | 0.000 | 0.000 | 0.004 | 0.004 | 0.019 | 0.019 | 2.819 | 7.935 |
| $S_3$ | 0.000 | 0.045 | 0.047 | **0.885** | 0.001 | 0.001 | 0.009 | 0.008 | 0.002 | 0.003 | 3.006 | 0.933 |
| $S_4$ | 0.000 | 0.005 | 0.005 | 0.016 | 0.007 | 0.008 | **0.480** | **0.456** | 0.012 | 0.012 | 3.282 | 1.833 |
| $S_5$ | 0.000 | 0.006 | 0.006 | 0.000 | 0.000 | 0.000 | **0.436** | **0.454** | 0.052 | 0.044 | 3.422 | 1.581 |
| $S_6$ | 0.000 | 0.025 | 0.025 | 0.000 | 0.000 | 0.000 | 0.052 | 0.060 | **0.425** | **0.413** | 3.583 | 0.413 |
| $S_7$ | 0.000 | 0.021 | 0.022 | 0.000 | 0.000 | 0.000 | 0.006 | 0.006 | **0.462** | **0.482** | 3.711 | 0.217 |
| $S_8$ | 0.001 | 0.000 | 0.000 | 0.000 | **0.508** | **0.484** | 0.003 | 0.002 | 0.001 | 0.001 | 4.436 | 0.020 |
| $S_9$ | 0.001 | 0.000 | 0.000 | 0.000 | **0.483** | **0.505** | 0.005 | 0.004 | 0.001 | 0.001 | 4.497 | 0.033 |
| $\mu^2_{0\to i(dia.)}$ (a.u.) | - | 16.363 | 16.198 | 0.006 | 0.074 | 0.085 | 1.947 | 1.882 | 1.144 | 1.118 | - | - |

## S3.2 Simulation of excited state dynamics

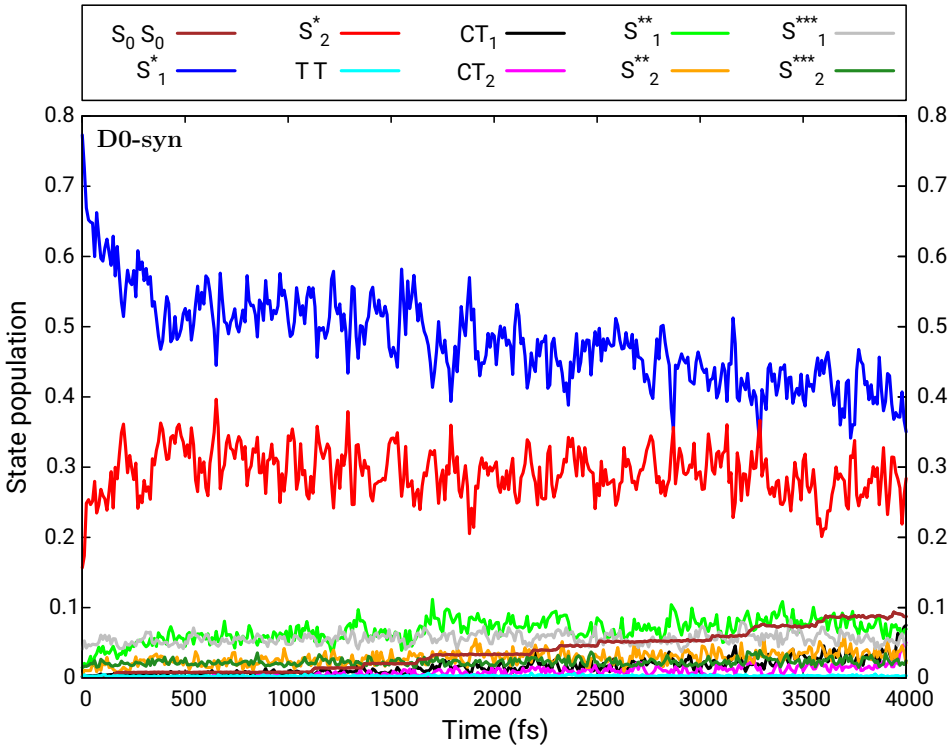


Figure S13: Excitonic state populations as functions of time for dimer **D0-syn** of ML-DPBF. The reported results are obtained by averaging over all trajectories and time intervals of 10 fs.

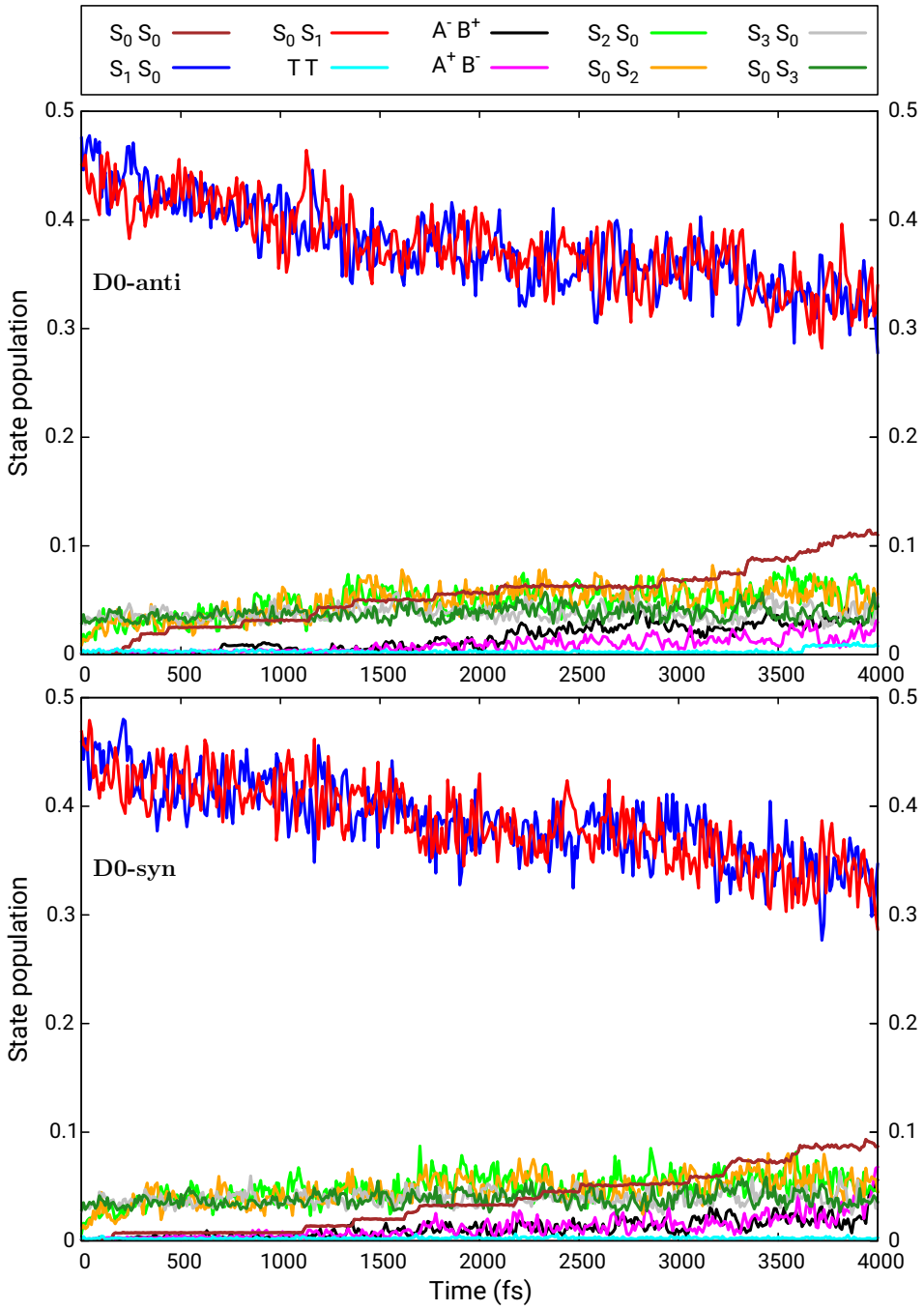


Figure S14: Diabatic state populations as functions of time for two conformers of dimer **D0** of ML-DPBF, namely **D0-anti** (upper panel) and **D0-syn** (lower panel). The reported results are obtained by averaging over all trajectories and time intervals of 10 fs.

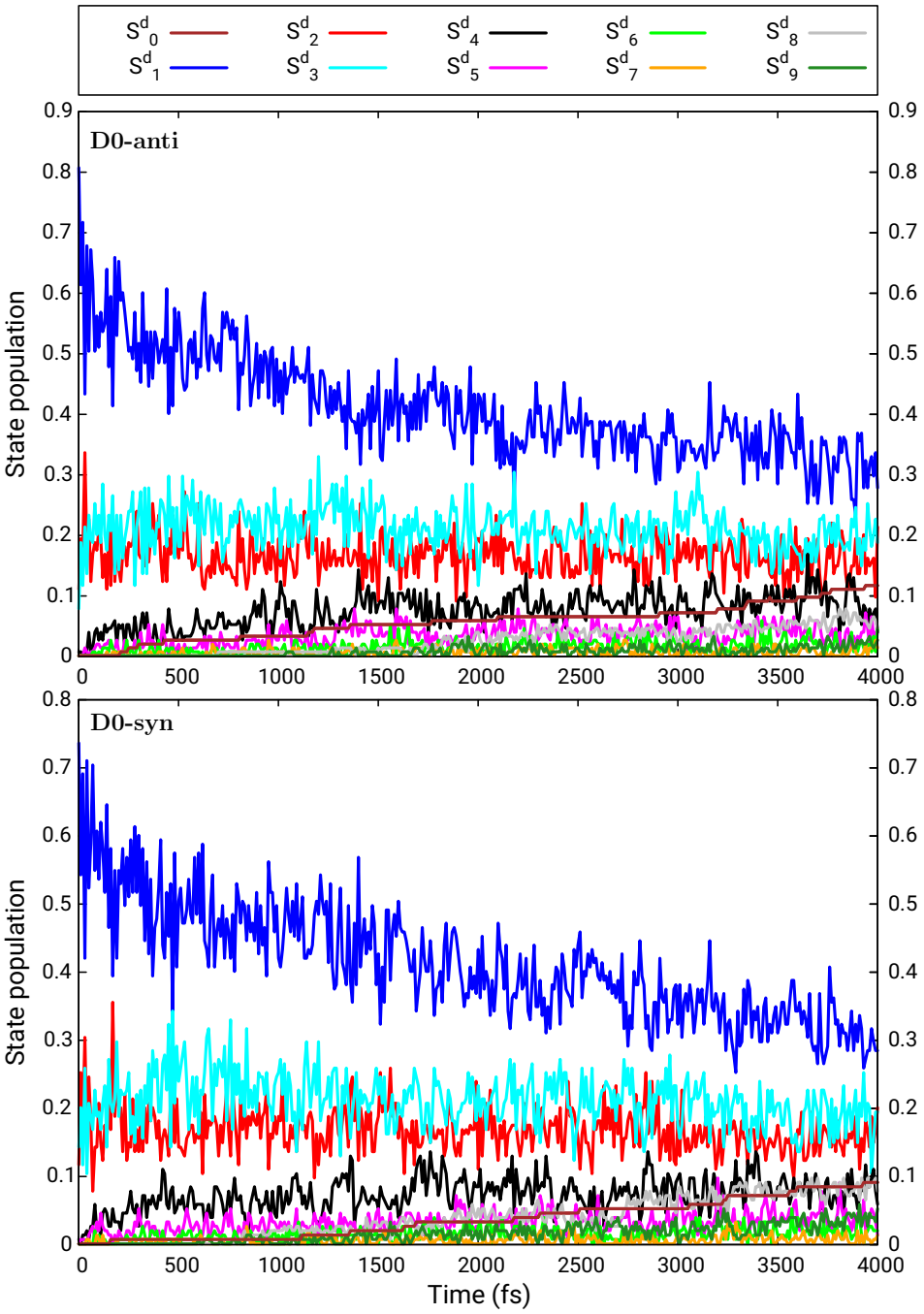


Figure S15: Adiabatic state populations as functions of time for two conformers of dimer **D0** of ML-DPBF, namely **D0-anti** (upper panel) and **D0-syn** (lower panel). A superscript $d$ is added to the state labels to indicate that they are the adiabatic states of the dimers. The reported results are obtained by averaging over all trajectories and time intervals of 10 fs.

Table S17: Average transition rates between pairs of excitonic states obtained in the simulations of the excited state dynamics for two conformers of dimer **D0** of ML-DPBF, namely **D0-anti** and **D0-syn**. The charge transfer states $CT_1$ and $CT_2$, the higher excitonic states $S_1^{**}$ and $S_2^{**}$, and $S_1^{***}$ and $S_2^{***}$ are grouped together and indicated as $CT$, $S^{**}$ and $S^{***}$, respectively. The complete list of state-to-state transition rates is provided in Table S18. Each rate, defined as $\frac{\#\ transitions}{\#\ trajectories\ \cdot\ time\ interval}$, is computed over the whole simulations (0-4 ps) and reported in units of ps$^{-1}$.

| States | | Dimer **D0-anti** Rates (ps$^{-1}$) | | | Dimer **D0-syn** Rates (ps$^{-1}$) | | |
|---|---|---|---|---|---|---|---|
| $i$ | $j$ | $i \rightarrow j$ | $j \rightarrow i$ | net[a] | $i \rightarrow j$ | $j \rightarrow i$ | net[a] |
| $S_1^*$ | $S_0S_0$ | 0.008 | 0.000 | 0.008 | 0.008 | 0.002 | 0.006 |
| $S_2^*$ | $S_0S_0$ | 0.008 | 0.002 | 0.006 | 0.002 | 0.002 | 0.000 |
| $TT$ | $S_0S_0$ | 0.000 | 0.000 | 0.000 | 0.000 | 0.000 | 0.000 |
| $CT$ | $S_0S_0$ | 0.000 | 0.000 | 0.000 | 0.000 | 0.000 | 0.000 |
| $S^{**}$ | $S_0S_0$ | 0.011 | 0.002 | 0.009 | 0.013 | 0.000 | 0.013 |
| $S^{***}$ | $S_0S_0$ | 0.006 | 0.002 | 0.004 | 0.003 | 0.000 | 0.003 |
| $S_2^*$ | $S_1^*$ | 12.090 | 11.142 | 0.948 | 12.447 | 11.503 | 0.944 |
| $TT$ | $S_1^*$ | 0.631 | 0.635 | -0.004 | 0.552 | 0.534 | 0.018 |
| $CT$ | $S_1^*$ | 0.000 | 0.021 | -0.021 | 0.000 | 0.019 | -0.019 |
| $S^{**}$ | $S_1^*$ | 0.965 | 1.700 | -0.735 | 0.998 | 1.676 | -0.678 |
| $S^{***}$ | $S_1^*$ | 0.174 | 0.495 | -0.321 | 0.169 | 0.555 | -0.386 |
| $TT$ | $S_2^*$ | 0.563 | 0.561 | 0.002 | 0.485 | 0.489 | -0.004 |
| $CT$ | $S_2^*$ | 0.000 | 0.002 | -0.002 | 0.002 | 0.005 | -0.003 |
| $S^{**}$ | $S_2^*$ | 8.623 | 7.468 | 1.155 | 8.523 | 7.342 | 1.181 |
| $S^{***}$ | $S_2^*$ | 0.756 | 0.898 | -0.142 | 0.745 | 0.929 | -0.184 |
| $CT$ | $TT$ | 0.000 | 0.000 | 0.000 | 0.000 | 0.002 | -0.002 |
| $S^{**}$ | $TT$ | 0.063 | 0.063 | 0.000 | 0.090 | 0.074 | 0.016 |
| $S^{***}$ | $TT$ | 0.003 | 0.005 | -0.002 | 0.006 | 0.006 | 0.000 |
| $S^{**}$ | $CT$ | 0.008 | 0.008 | 0.000 | 0.008 | 0.002 | 0.006 |
| $S^{***}$ | $CT$ | 0.023 | 0.026 | -0.003 | 0.035 | 0.034 | 0.001 |
| $S^{***}$ | $S^{**}$ | 4.474 | 4.024 | 0.450 | 4.427 | 3.866 | 0.561 |

[a] Difference between the $i \rightarrow j$ rate and the $j \rightarrow i$ one.

Table S18: Average transition rates between pairs of excitonic states obtained in the simulations of the excited state dynamics for two conformers of dimer **D0** of ML-DPBF, namely **D0-anti** and **D0-syn**. Each rate, defined as $\frac{\#\ transitions}{\#\ trajectories\ \cdot\ time\ interval}$, is computed over the whole simulations (0-4 ps) and reported in units of ps$^{-1}$.

| States | | Dimer **D0-anti** Rates (ps$^{-1}$) | | | Dimer **D0-syn** Rates (ps$^{-1}$) | | |
|---|---|---|---|---|---|---|---|
| $i$ | $j$ | $i \rightarrow j$ | $j \rightarrow i$ | net[a] | $i \rightarrow j$ | $j \rightarrow i$ | net[a] |
| $S_1^*$ | $S_0S_0$ | 0.008 | 0.000 | 0.008 | 0.008 | 0.002 | 0.006 |
| $S_2^*$ | $S_0S_0$ | 0.008 | 0.002 | 0.006 | 0.002 | 0.002 | 0.000 |
| $TT$ | $S_0S_0$ | 0.000 | 0.000 | 0.000 | 0.000 | 0.000 | 0.000 |
| $CT_1$ | $S_0S_0$ | 0.000 | 0.000 | 0.000 | 0.000 | 0.000 | 0.000 |
| $CT_2$ | $S_0S_0$ | 0.000 | 0.000 | 0.000 | 0.000 | 0.000 | 0.000 |
| $S_1^{**}$ | $S_0S_0$ | 0.008 | 0.002 | 0.006 | 0.010 | 0.000 | 0.010 |
| $S_2^{**}$ | $S_0S_0$ | 0.003 | 0.000 | 0.003 | 0.003 | 0.000 | 0.003 |
| $S_1^{***}$ | $S_0S_0$ | 0.005 | 0.002 | 0.003 | 0.003 | 0.000 | 0.003 |
| $S_2^{***}$ | $S_0S_0$ | 0.002 | 0.000 | 0.002 | 0.000 | 0.000 | 0.000 |
| $S_2^*$ | $S_1^*$ | 12.090 | 11.142 | 0.948 | 12.447 | 11.503 | 0.944 |
| $TT$ | $S_1^*$ | 0.631 | 0.635 | -0.004 | 0.552 | 0.534 | 0.018 |
| $CT_1$ | $S_1^*$ | 0.000 | 0.002 | -0.002 | 0.000 | 0.005 | -0.005 |
| $CT_2$ | $S_1^*$ | 0.000 | 0.019 | -0.019 | 0.000 | 0.015 | -0.015 |
| $S_1^{**}$ | $S_1^*$ | 0.797 | 1.289 | -0.492 | 0.855 | 1.289 | -0.434 |
| $S_2^{**}$ | $S_1^*$ | 0.168 | 0.411 | -0.243 | 0.144 | 0.387 | -0.243 |
| $S_1^{***}$ | $S_1^*$ | 0.144 | 0.374 | -0.230 | 0.132 | 0.432 | -0.300 |
| $S_2^{***}$ | $S_1^*$ | 0.031 | 0.121 | -0.090 | 0.037 | 0.123 | -0.086 |
| $TT$ | $S_2^*$ | 0.563 | 0.561 | 0.002 | 0.485 | 0.489 | -0.004 |
| $CT_1$ | $S_2^*$ | 0.000 | 0.000 | 0.000 | 0.000 | 0.000 | 0.000 |
| $CT_2$ | $S_2^*$ | 0.000 | 0.002 | -0.002 | 0.002 | 0.005 | -0.003 |
| $S_1^{**}$ | $S_2^*$ | 8.210 | 6.750 | 1.460 | 8.129 | 6.661 | 1.468 |
| $S_2^{**}$ | $S_2^*$ | 0.413 | 0.718 | -0.305 | 0.394 | 0.681 | -0.287 |
| $S_1^{***}$ | $S_2^*$ | 0.708 | 0.735 | -0.027 | 0.710 | 0.721 | -0.011 |
| $S_2^{***}$ | $S_2^*$ | 0.048 | 0.163 | -0.115 | 0.035 | 0.208 | -0.173 |
| $CT_1$ | $TT$ | 0.000 | 0.000 | 0.000 | 0.000 | 0.000 | 0.000 |
| $CT_2$ | $TT$ | 0.000 | 0.000 | 0.000 | 0.000 | 0.002 | -0.002 |
| $S_1^{**}$ | $TT$ | 0.063 | 0.061 | 0.002 | 0.089 | 0.074 | 0.015 |
| $S_2^{**}$ | $TT$ | 0.000 | 0.002 | -0.002 | 0.002 | 0.000 | 0.002 |
| $S_1^{***}$ | $TT$ | 0.003 | 0.005 | -0.002 | 0.005 | 0.006 | -0.001 |
| $S_2^{***}$ | $TT$ | 0.000 | 0.000 | 0.000 | 0.002 | 0.000 | 0.002 |
| $CT_2$ | $CT_1$ | 0.521 | 0.503 | 0.018 | 0.556 | 0.542 | 0.014 |
| $S_1^{**}$ | $CT_1$ | 0.002 | 0.005 | -0.003 | 0.000 | 0.000 | 0.000 |
| $S_2^{**}$ | $CT_1$ | 0.000 | 0.000 | 0.000 | 0.000 | 0.000 | 0.000 |
| $S_1^{***}$ | $CT_1$ | 0.002 | 0.000 | 0.002 | 0.000 | 0.002 | -0.002 |
| $S_2^{***}$ | $CT_1$ | 0.005 | 0.011 | -0.006 | 0.018 | 0.016 | 0.002 |
| $S_1^{**}$ | $CT_2$ | 0.006 | 0.002 | 0.004 | 0.008 | 0.002 | 0.006 |
| $S_2^{**}$ | $CT_2$ | 0.000 | 0.002 | -0.002 | 0.000 | 0.000 | 0.000 |
| $S_1^{***}$ | $CT_2$ | 0.003 | 0.003 | 0.000 | 0.003 | 0.000 | 0.003 |
| $S_2^{***}$ | $CT_2$ | 0.013 | 0.011 | 0.002 | 0.015 | 0.016 | -0.001 |
| $S_2^{**}$ | $S_1^{**}$ | 2.826 | 1.987 | 0.839 | 2.719 | 1.913 | 0.806 |
| $S_1^{***}$ | $S_1^{**}$ | 2.039 | 1.887 | 0.152 | 2.195 | 1.885 | 0.310 |
| $S_2^{***}$ | $S_1^{**}$ | 0.056 | 0.058 | -0.002 | 0.060 | 0.092 | -0.032 |
| $S_1^{***}$ | $S_2^{**}$ | 2.100 | 1.760 | 0.340 | 1.852 | 1.574 | 0.278 |
| $S_2^{***}$ | $S_2^{**}$ | 0.279 | 0.319 | -0.040 | 0.321 | 0.315 | 0.006 |
| $S_2^{***}$ | $S_1^{***}$ | 0.737 | 0.489 | 0.248 | 0.739 | 0.458 | 0.281 |

[a] Difference between the $i \rightarrow j$ rate and the $j \rightarrow i$ one.

Figure S16: Net transition rates (in $ps^{-1}$) between pairs of states as functions of time (fs), obtained from the simulation of the excited state dynamics for dimer **D0-anti** of ML-DPBF. The higher excitonic states $S_1^{**}$ and $S_2^{**}$, and $S_1^{***}$ and $S_2^{***}$ are grouped together and indicated as $S^{**}$ and $S^{***}$, respectively. Each rate is defined as $\frac{\#\ transitions}{\#\ trajectories\ \cdot\ time\ interval}$. For each type of transition, one bar represents a net transition rate computed in a time interval of 25 fs (e.g. the first bar corresponds to the interval $(0{:}25]$ fs).

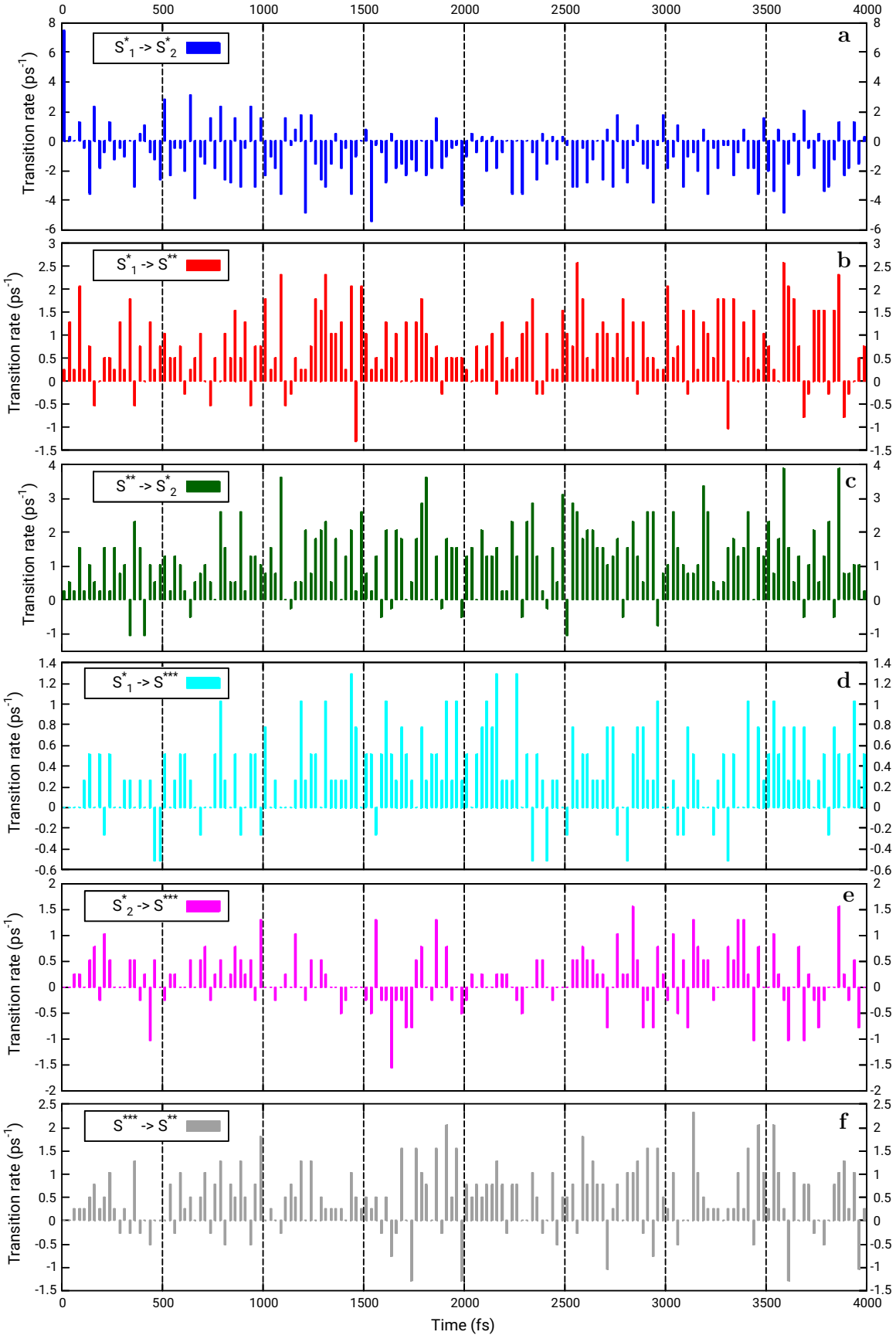

Table S19: Average values (diagonal and lower triangular part) and standard deviations (upper triangular part) of the electronic Hamiltonian matrix elements in the excitonic basis at the geometries where the current adiabatic wavefunction is dominated by the excitonic $S_1^*$ state, obtained from the simulations of the excited state dynamics for two conformers of dimer **D0** of ML-DPBF, namely **D0-anti** and **D0-syn**.

Dimer **D0-anti**

| $\hat{\mathcal{H}}_{el}$ | $S_0S_0$ | $S_1^*$ | $S_2^*$ | $TT$ | $CT_1$ | $CT_2$ | $S_1^{**}$ | $S_2^{**}$ | $S_1^{***}$ | $S_2^{***}$ |
|---|---|---|---|---|---|---|---|---|---|---|
| $S_0S_0$ | 0.00 | ± 59.55 | ± 49.66 | ± 3.59 | ± 343.71 | ± 39.23 | ± 91.41 | ± 63.30 | ± 59.14 | ± 43.51 |
| $S_1^*$ | -0.06 | 2500.05 | ± 0.00 | ± 0.58 | ± 51.71 | ± 18.06 | ± 98.30 | ± 49.81 | ± 202.53 | ± 98.92 |
| $S_2^*$ | 0.22 | 0.00 | 2760.70 | ± 0.25 | ± 15.04 | ± 10.09 | ± 37.87 | ± 57.87 | ± 70.55 | ± 164.21 |
| $TT$ | 0.00 | 0.00 | 0.00 | 2579.93 | ± 20.27 | ± 27.90 | ± 2.43 | ± 0.70 | ± 1.45 | ± 0.80 |
| $CT_1$ | -4.12 | 0.06 | 0.01 | 0.02 | 3952.50 | ± 0.00 | ± 217.65 | ± 38.64 | ± 122.95 | ± 13.33 |
| $CT_2$ | -0.07 | -0.01 | -0.02 | 0.00 | 0.00 | 4122.75 | ± 31.20 | ± 10.78 | ± 17.31 | ± 10.99 |
| $S_1^{**}$ | -0.47 | 0.36 | -0.10 | 0.00 | 0.94 | 0.10 | 3030.20 | ± 0.00 | ± 46.50 | ± 22.52 |
| $S_2^{**}$ | 0.06 | 0.06 | 0.04 | 0.00 | 0.00 | -0.03 | 0.00 | 3296.58 | ± 21.78 | ± 30.29 |
| $S_1^{***}$ | 0.18 | -0.07 | 0.04 | 0.00 | 0.34 | -0.03 | 0.21 | -0.04 | 3261.74 | ± 0.00 |
| $S_2^{***}$ | 0.09 | -0.08 | 0.17 | 0.00 | -0.03 | -0.05 | 0.02 | -0.05 | 0.00 | 3561.98 |

Dimer **D0-syn**

| $\hat{\mathcal{H}}_{el}$ | $S_0S_0$ | $S_1^*$ | $S_2^*$ | $TT$ | $CT_1$ | $CT_2$ | $S_1^{**}$ | $S_2^{**}$ | $S_1^{***}$ | $S_2^{***}$ |
|---|---|---|---|---|---|---|---|---|---|---|
| $S_0S_0$ | 0.00 | ± 58.28 | ± 47.78 | ± 4.53 | ± 371.07 | ± 38.12 | ± 93.75 | ± 59.85 | ± 59.67 | ± 40.97 |
| $S_1^*$ | -0.08 | 2498.29 | ± 0.00 | ± 0.71 | ± 54.52 | ± 20.08 | ± 96.30 | ± 48.68 | ± 200.78 | ± 97.50 |
| $S_2^*$ | 0.08 | 0.00 | 2755.32 | ± 0.30 | ± 16.99 | ± 11.12 | ± 37.75 | ± 57.08 | ± 69.38 | ± 162.75 |
| $TT$ | -0.01 | 0.00 | 0.00 | 2579.19 | ± 23.13 | ± 31.12 | ± 3.07 | ± 0.77 | ± 1.71 | ± 0.64 |
| $CT_1$ | -1.37 | 0.04 | -0.01 | -0.09 | 3950.35 | ± 0.00 | ± 235.88 | ± 51.59 | ± 131.62 | ± 13.44 |
| $CT_2$ | 0.04 | 0.02 | 0.02 | 0.01 | 0.00 | 4138.52 | ± 30.77 | ± 9.92 | ± 16.46 | ± 8.85 |
| $S_1^{**}$ | -0.48 | 0.30 | 0.01 | -0.01 | 1.17 | 0.04 | 3037.84 | ± 0.00 | ± 46.48 | ± 21.11 |
| $S_2^{**}$ | 0.03 | 0.11 | 0.08 | 0.00 | -0.17 | 0.00 | 0.00 | 3294.79 | ± 21.40 | ± 29.69 |
| $S_1^{***}$ | 0.29 | -0.01 | 0.17 | -0.01 | 0.67 | 0.07 | 0.39 | 0.05 | 3257.63 | ± 0.00 |
| $S_2^{***}$ | 0.04 | -0.21 | -0.14 | 0.00 | -0.01 | -0.04 | 0.03 | 0.03 | 0.00 | 3556.85 |

Table S20: Average values (diagonal and lower triangular part) and standard deviations (upper triangular part) of the electronic Hamiltonian matrix elements in the excitonic basis at the geometries where the current adiabatic wavefunction is dominated by the excitonic $S_2^*$ state, obtained from the simulations of the excited state dynamics for two conformers of dimer **D0** of ML-DPBF, namely **D0-anti** and **D0-syn**.

Dimer **D0-anti**

| $\hat{\mathcal{H}}_{el}$ | $S_0S_0$ | $S_1^*$ | $S_2^*$ | $TT$ | $CT_1$ | $CT_2$ | $S_1^{**}$ | $S_2^{**}$ | $S_1^{***}$ | $S_2^{***}$ |
|---|---|---|---|---|---|---|---|---|---|---|
| $S_0S_0$ | 0.00 | ± 51.85 | ± 50.87 | ± 2.62 | ± 254.35 | ± 35.74 | ± 78.76 | ± 68.28 | ± 54.87 | ± 37.52 |
| $S_1^*$ | -0.23 | 2541.37 | ± 0.00 | ± 0.43 | ± 36.34 | ± 17.04 | ± 88.74 | ± 53.58 | ± 192.80 | ± 116.07 |
| $S_2^*$ | 0.16 | 0.00 | 2748.13 | ± 0.20 | ± 12.01 | ± 8.31 | ± 42.79 | ± 59.46 | ± 87.12 | ± 157.99 |
| $TT$ | 0.00 | 0.00 | 0.00 | 2583.41 | ± 21.68 | ± 28.77 | ± 1.71 | ± 0.65 | ± 1.14 | ± 0.65 |
| $CT_1$ | 0.86 | 0.11 | -0.01 | 0.07 | 4032.18 | ± 0.00 | ± 150.84 | ± 33.40 | ± 96.16 | ± 12.46 |
| $CT_2$ | -0.17 | -0.06 | 0.03 | -0.03 | 0.00 | 4153.91 | ± 25.89 | ± 10.16 | ± 16.66 | ± 10.98 |
| $S_1^{**}$ | -0.06 | 0.18 | -0.06 | 0.01 | 0.24 | 0.15 | 3059.54 | ± 0.00 | ± 42.48 | ± 21.99 |
| $S_2^{**}$ | 0.01 | -0.06 | 0.22 | 0.00 | 0.10 | 0.00 | 0.00 | 3266.40 | ± 24.88 | ± 31.28 |
| $S_1^{***}$ | 0.17 | 0.47 | -0.11 | 0.00 | 0.18 | 0.05 | 0.39 | 0.08 | 3304.43 | ± 0.00 |
| $S_2^{***}$ | 0.09 | -0.37 | -0.13 | 0.00 | -0.02 | -0.05 | 0.02 | 0.06 | 0.00 | 3533.07 |

Dimer **D0-syn**

| $\hat{\mathcal{H}}_{el}$ | $S_0S_0$ | $S_1^*$ | $S_2^*$ | $TT$ | $CT_1$ | $CT_2$ | $S_1^{**}$ | $S_2^{**}$ | $S_1^{***}$ | $S_2^{***}$ |
|---|---|---|---|---|---|---|---|---|---|---|
| $S_0S_0$ | 0.00 | ± 51.11 | ± 49.74 | ± 3.21 | ± 275.26 | ± 35.48 | ± 79.34 | ± 65.45 | ± 54.72 | ± 35.33 |
| $S_1^*$ | 0.01 | 2542.64 | ± 0.00 | ± 0.54 | ± 40.20 | ± 18.82 | ± 87.02 | ± 53.19 | ± 190.93 | ± 115.06 |
| $S_2^*$ | -0.02 | 0.00 | 2743.20 | ± 0.24 | ± 13.44 | ± 8.71 | ± 42.29 | ± 58.60 | ± 86.12 | ± 156.82 |
| $TT$ | 0.00 | 0.00 | 0.00 | 2583.56 | ± 24.57 | ± 32.20 | ± 2.08 | ± 0.69 | ± 1.30 | ± 0.56 |
| $CT_1$ | -1.13 | 0.00 | 0.04 | 0.00 | 4042.17 | ± 0.00 | ± 163.42 | ± 44.49 | ± 102.43 | ± 14.03 |
| $CT_2$ | 0.11 | -0.01 | -0.02 | -0.06 | 0.00 | 4170.76 | ± 25.62 | ± 10.09 | ± 16.24 | ± 8.91 |
| $S_1^{**}$ | -0.05 | 0.01 | -0.16 | 0.00 | 0.78 | 0.07 | 3064.98 | ± 0.00 | ± 41.53 | ± 20.52 |
| $S_2^{**}$ | 0.12 | 0.08 | -0.02 | 0.00 | 0.00 | 0.00 | 0.00 | 3263.42 | ± 24.55 | ± 30.59 |
| $S_1^{***}$ | 0.07 | -0.06 | -0.29 | 0.00 | -0.09 | 0.02 | 0.25 | 0.05 | 3302.51 | ± 0.00 |
| $S_2^{***}$ | 0.02 | 0.27 | -0.35 | 0.00 | -0.07 | 0.02 | -0.01 | 0.13 | 0.00 | 3527.44 |

## S3.3 Fitting of the state populations

In order to extract the state lifetimes, we fitted the populations obtained in the nonadiabatic simulations for dimer **D0** using the following rate model:

$$X \xrightarrow{1/\tau_{xy},\, 1/\tau'_{xy}} Y \xrightarrow{1/\tau_{yz}} Z \tag{S25}$$

where $\tau_{xy}$, $\tau'_{xy}$ and $\tau_{yz}$ are time constants, and $X$, $Y$ and $Z$ are (groups of) diabatic states, namely $X = S_1^*$, $Y = S_2^*, CT, S^{**}, S^{***}$ and $Z = TT, S_0S_0$. In particular, the decay of the initially populated $X$ state was modelled by a biexponential function:

$$P_X(t) = P_X(0)\,[\, w\, e^{-t/\tau_{xy}} + (1-w)\, e^{-t/\tau'_{xy}}\,] \tag{S26}$$

in which $P_X(0)$ is the initial population of state $X$ and $w$ is a constant between 0 and 1. Assuming a monoexponential decay of the group of intermediate states $Y$, its population was then fitted using the following function:

$$P_Y(t) = f_{xy}\, e^{-t/\tau_{xy}} + f'_{xy}\, e^{-t/\tau'_{xy}} + f_{yz}\, e^{-t/\tau_{yz}} \tag{S27}$$

where $f_{xy} = P_X(0)\; w\; \frac{\tau_{yz}}{\tau_{xy}-\tau_{yz}}$, $f'_{xy} = P_X(0)\;(1-w)\;\frac{\tau_{yz}}{\tau'_{xy}-\tau_{yz}}$ and $f_{yz} = P_Y(0) - f_{xy} - f'_{xy}$. Since the sum of the populations is equal to 1 at each time, we have:

$$P_Z(t) = 1 - P_X(t) - P_Y(t). \tag{S28}$$

In the fitting procedure, we started from the known initial populations $P_X(0)$ and $P_Y(0)$, namely 0.881 and 0.119 for **D0-anti**, and 0.845 and 0.154 for **D0-syn**; then, we determined $\tau_{xy}$, $\tau'_{xy}$ and $w$ by fitting $P_X(t)$, while $\tau_{yz}$ was extracted by subsequently fitting $P_Y(t)$. In this way we obtained $\tau_{xy}$ = 0.03 ps, $\tau'_{xy}$ = 10.4 ps, $\tau_{yz}$ = 17.3 ps and $w$ = 0.360 for **D0-anti**, and $\tau_{xy}$ = 0.04 ps, $\tau'_{xy}$ = 11.6 ps, $\tau_{yz}$ = 23.5 ps and $w$ = 0.334 for **D0-syn**, which define the fitting functions shown in Figure S17.

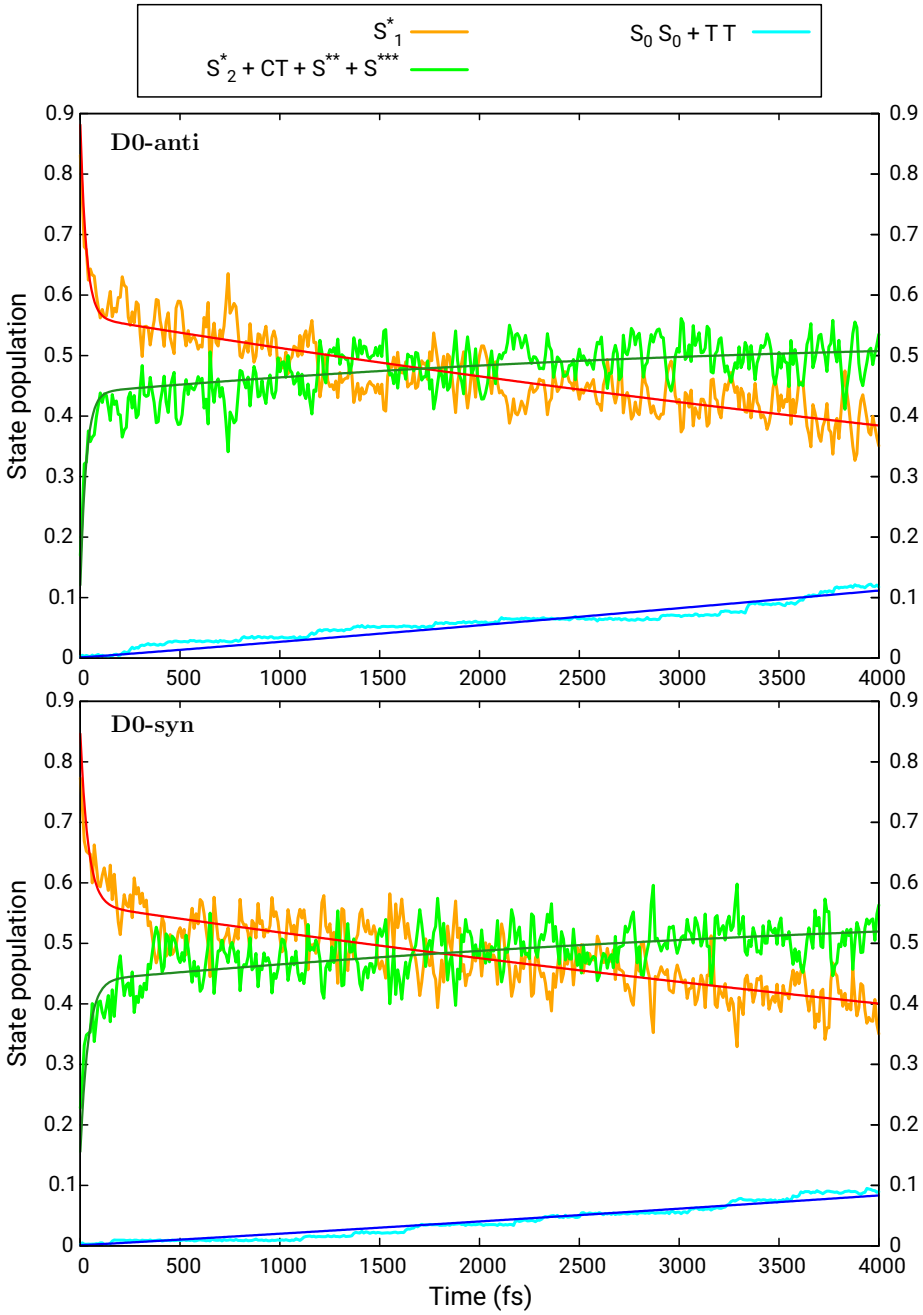


Figure S17: Excitonic state populations of dimer **D0** fitted by the rate model of Eq. S25. Upper panel, conformer **D0-anti**; lower panel, **D0-syn**. Fitting functions: red line, Eq. S26; green line, Eq. S27; blue line, Eq. S28.

# References


[1] A. F. Schwerin, J. C. Johnson, M. B. Smith, P. Sreearunothai, D. Popović, J. Černý, Z. Havias, I. Paci, A. Akdag, M. K. MacLeod, X. Chen, D. E. David, M. A. Ratner, J. R. Miller, A. J. Nozik, and J. Michl. Toward designed singlet fission: Electronic states and photophysics of 1,3-diphenylisobenzofuran. *J. Phys. Chem. A*, 114(3):1457–1473, 2010.

[2] W.G. Herkstroeter and P.B. Merkel. The triplet state energies of rubrene and diphenylisobenzofuran. *J. Photochem.*, 16(4):331–341, 1981.

[3] The OPLS-AA Lennard-Jones (or van der Waals) parameters were taken from those distributed with the TINKER 6.3 package, which in turn are from "OPLS All-Atom parameters for Organic Molecules, Ions, Peptides and Nucleic Acids, July 2008" as provided by W. L. Jorgensen, Yale University during June 2009.

[4] P. Jørgensen and J. Simons. Second quantization-based methods in quantum chemistry. *Academic Press, New York*, 1981.

[5] C. de Graaf and R. Broer. Magnetic interactions in molecules and solids. *Springer*, 2015.

[6] P.-O. Löwdin. On the Nonorthogonality Problem. *Adv. Quant. Chem.*, 5(C): 185–199, 1970.

[7] G. Granucci, M. Persico, and A. Toniolo. Direct semiclassical simulation of photochemical processes with semiempirical wave functions. *J. Chem. Phys.*, 114(24):10608–10615, 2001.

[8] L. Verlet. Computer "experiments" on classical fluids. I. Thermodynamical properties of Lennard-Jones molecules. *Phys. Rev.*, 159:98–103, 1967.

[9] G. Stock and M. Thoss. Classical description of nonadiabatic quantum dynamics. In *Advances in Chemical Physics*, chapter 5, pages 243–375. John Wiley & Sons, Ltd, 2005.

[10] R. Crespo-Otero and M. Barbatti. Recent advances and perspectives on nonadiabatic mixed quantum-classical dynamics. *Chem. Rev.*, 118(15):7026–7068, 2018.

[11] J. C. Tully. Molecular dynamics with electronic transitions. *J. Chem. Phys.*, 93 (2):1061–1071, 1990.

[12] F. Plasser, G. Granucci, J. Pittner, M. Barbatti, M. Persico, and H. Lischka. Surface hopping dynamics using a locally diabatic formalism: Charge transfer in the ethylene dimer cation and excited state dynamics in the 2-pyridone dimer. *J. Chem. Phys.*, 137(22):22A514, 2012.

[13] S. Mai, P. Marquetand, and L. González. Nonadiabatic dynamics: The sharc approach. *WIREs Comput. Mol. Sci.*, 8(6):e1370, 2018.

[14] N. Aguilera-Porta, I. Corral, J. Munoz-Muriedas, and G. Granucci. Excited state dynamics of some nonsteroidal anti-inflammatory drugs: A surface-hopping investigation. *Comput. Theor. Chem.*, 1152:20–27, 2019.

[15] L. Creatini, T. Cusati, G. Granucci, and M. Persico. Photodynamics of azobenzene in a hindering environment. *Chem. Phys.*, 347:492–502, 2008.

[16] M. Persico and G. Granucci. An overview of nonadiabatic dynamics simulations methods, with focus on the direct approach versus the fitting of potential energy surfaces. *Theor. Chem. Acc.*, 133:1526/1–1526/28, 2014.

[17] M. Born and K. Huang. Dynamical Theory of Crystal Lattices. *Clarendon, Oxford*, 1954.

[18] L. Wang, A. Akimov, and O. V. Prezhdo. Recent progress in surface hopping: 2011-2015. *J. Phys. Chem. Lett.*, 7(11):2100–2112, 2016.

[19] J. E. Subotnik, A. Jain, B. Landry, A. Petit, W. Ouyang, and N. Bellonzi. Understanding the surface hopping view of electronic transitions and decoherence. *Annual Rev. Phys. Chem.*, 67(1):387–417, 2016.

[20] G. Granucci, M. Persico, and Zoccante A. Including quantum decoherence in surface hopping. *J. Chem. Phys.*, 133:134111/1–134111/9, 2010.

[21] G. Granucci and A. Toniolo. Molecular gradients for semiempirical CI wavefunctions with floating occupation molecular orbitals. *Chem. Phys. Lett.*, 325: 79–85, 2000.

[22] M. J. S. Dewar, E. G. Zoebisch, E. F. Healy, and J. J. P. Stewart. AM1: a new general purpose quantum mechanical molecular model. *J. Am. Chem. Soc.*, 107 (13):3902–3909, 1985.

[23] W. F. van Gunsteren and H. J. C. Berendsen. Algorithms for brownian dynamics. *Mol. Phys.*, 45(3):637–647, 1982.